haematologica
Journal of the Ferrata Storti Foundation

Immunogenomic characterization of classic Hodgkin lymphoma variant of Richter transformation reveals shared biology with *de novo* classic Hodgkin lymphoma

by Mingfei Yan, Sameer A. Parikh, Michelly K. Sampaio De Melo, Paul J. Hampel, Nathaniel Aleynick, Alexander Chan, Ozgur Can Eren, Katherine Lopez, Alexa Cohen, Mikhail Roshal, Megan S. Lim, Leonardo Boiocchi, Ahmet Dogan, Yanming Zhang, Sutapa Sinha, Kari G. Rabe, Neil E. Kay, Elaine S. Jaffe, Rebecca L. King and Wenbin Xiao

Received: August 8, 2026.
Accepted: October 23, 2026.

Citation: Mingfei Yan, Sameer A. Parikh, Michelly K. Sampaio De Melo, Paul J. Hampel, Nathaniel Aleynick, Alexander Chan, Ozgur Can Eren, Katherine Lopez, Alexa Cohen, Mikhail Roshal, Megan S. Lim, Leonardo Boiocchi, Ahmet Dogan, Yanming Zhang, Sutapa Sinha, Kari G. Rabe, Neil E. Kay, Elaine S. Jaffe, Rebecca L. King and Wenbin Xiao. Immunogenomic characterization of classic Hodgkin lymphoma variant of Richter transformation reveals shared biology with de novo classic Hodgkin lymphoma. Haematologica. 2026 Oct 29. doi: 10.3324/haematol.2026.301780 [Epub ahead of print]

Publisher's Disclaimer.
E-publishing ahead of print is increasingly important for the rapid dissemination of science. Haematologica is, therefore, E-publishing PDF files of an early version of manuscripts that have completed a regular peer review and have been accepted for publication.
E-publishing of this PDF file has been approved by the authors.
After having E-published Ahead of Print, manuscripts will then undergo technical and English editing, typesetting, proof correction and be presented for the authors' final approval, the final version of the manuscript will then appear in a regular issue of the journal.
All legal disclaimers that apply to the journal also pertain to this production process.

Immunogenomic characterization of classic Hodgkin lymphoma variant of Richter transformation reveals shared biology with *de novo* classic Hodgkin lymphoma

Mingfei Yan[1,&], Sameer A. Parikh[2,#], Michelly K. Sampaio De Melo[3,#], Paul J. Hampel[2], Nathaniel Aleynick[1], Alexander Chan[1], Ozgur Can Eren[1], Katherine Lopez[1], Alexa Cohen[1], Mikhail Roshal[1], Megan S. Lim[1], Leonardo Boiocchi[1], Ahmet Dogan[1], Yanming Zhang[1], Sutapa Sinha[2], Kari G. Rabe[2,4], Neil E. Kay[2,5], Elaine S. Jaffe[3,$], Rebecca L. King[6,$], Wenbin Xiao[1,*]

1. Department of Pathology and Laboratory Medicine, Memorial Sloan Kettering Cancer Center, New York, NY

2. Division of Hematology, Department of Medicine, Mayo Clinic, Rochester, MN

3. Laboratory of Pathology, Center for Cancer Research, National Cancer Institute, Bethesda, MD

4. Department of Quantitative Health Sciences, Division of Clinical Trials and Biostatistics, Mayo Clinic, Rochester, MN

5. Department of Immunology, Mayo Clinic, Rochester, MN

6. Department of Laboratory Medicine and Pathology, Mayo Clinic, Rochester, MN

#These authors contribute equally

$These authors contribute equally

& Current address: Department of Pathology and Laboratory Medicine, H. Lee Moffitt Cancer Center & Research Institute, Tampa, FL

Running title: cHL Variant Richter Transformation Shares *De Novo* cHL Biology

***Corresponding author:**

Wenbin Xiao, MD, PhD
Email: xiaow@mskcc.org

Funding:

This research was funded in part by the NIH and National Cancer Institute (NCI) Cancer Center Support Grant (P30 CA008748). W.X. is supported by a Cycle for Survival's Equinox Innovation Award in Rare Cancers and American Cancer Society LEAP award as well as MSK Leukemia SPORE (Career Enhancement Program; NIH/NCI P50 CA254838) and NIH/NCI grant (K08CA267058 and R37CA301130). We thank the Henry J. Predolin Foundation for their generous support of the Mayo Clinic CLL Tissue Bank. The work was also supported by Michael W. and Georgia Taylor Michelson. This

research was supported in part by the Intramural Research Program of the National Institutes of Health (NIH). The contributions of the NIH author(s) were made as part of their official duties as NIH federal employees, are in compliance with agency policy requirements, and are considered Works of the United States Government. However, the findings and conclusions presented in this paper are those of the author(s) and do not necessarily reflect the views of the NIH or the U.S. Department of Health and Human Services.

Conflict of Interest Disclosure:

W.X. has received research support from Stemline Therapeutics. Research funding for S.A.P has been provided to the institution from Janssen, AstraZeneca, BeOne, Merck, and Genentech for clinical studies in which S.A.P is a principal investigator; honoraria has been provided to the institution from Pharmacyclics, Merck, AstraZeneca, Janssen, BeOne, Genentech, SoBi, MingSight Pharmaceuticals, Novalgen Limited, Kite Pharma, and AbbVie for S.A.P's participation in consulting activities/advisory board meetings; S.A.P has also on the Data Safety Monitoring Committee for Merck. N.E.K. has served on advisory boards for AbbVie, AstraZeneca, BeiGene, Janssen, and Pharmacyclics, and on Data Safety Monitoring Committees (DSMCs) for AstraZeneca, BMS-Celgene, and Dren Bio; he has received research funding from AbbVie, Acerta Pharma, AstraZeneca, Genentech, Pharmacyclics/Janssen, and Merck; all research funding is provided directly to Mayo Clinic and is not received personally.

Acknowledgment:

We would like to thank Ms. Irina Linkov (Core facility, MSKCC) for providing technical support in performing immunohistochemical study.

Author Contributions:

M.Y., S.A.P., M.S.D.M., E.S.J., R.K., and W.X. collected and reviewed cases. P.J.H., K.L., A. Cohen, S.S., K.G.R., and N.E.K. collected data. N.A., M.S.L., L.B., and A.D. performed and analyzed multiplexed immunofluorescence data. A. Chan., O.C.E., and M.R. performed and analyzed flow cytometric data. Y.Z. performed and analyzed FISH studies. M.Y. and W.X. analyzed all the data and drafted the manuscript. W.X. conceived and supervised the study and provided research support.

Data-sharing Statement:

Original data can be shared upon request by contacting the corresponding author xiaow@mskcc.org.

Declaration of AI use: Generative AI was not used for all scientific content, analyses, interpretations, and conclusions of the study.

ABSTRACT

Richter transformation of chronic lymphocytic leukemia/small lymphocytic lymphoma (CLL/SLL) into classic Hodgkin lymphoma (CHL-RT) is rare and remains incompletely understood. Two histologic subtypes are recognized: type 1 (CLL/SLL with scattered Hodgkin/Reed-Sternberg (HRS) cells) and type 2 (HRS cells within a polymorphous inflammatory background). Previous studies suggest that type 1 represents an earlier stage of type 2 and that both may be clonally related to the underlying CLL/SLL. However, the immune evasion phenotype of HRS cells in CHL-RT and the genetic features of precursor CLL/SLL remain incompletely defined. In this multi-institutional study of 77 patients with CHL-RT (27 type 1 and 50 type 2), we characterized immune evasion markers, *PD-L1*/*PD-L2* copy number alterations, tumor microenvironment, and performed targeted next-generation sequencing on 37 CLL/SLL samples. HRS cells in both CHL-RT subtypes showed immune evasion features largely resembling *de novo* CHL. However, PD-L1 expression was less frequent in type 1 than type 2 CHL-RT (53.3% vs. 100%, $p<0.001$) and *de novo* CHL (85.7%, $p=0.009$). Gain/polysomy of *PD-L1/PD-L2* was common (83.3%), whereas amplification was uncommon (8.3%). Type 2 CHL-RT demonstrated a suppressive tumor microenvironment enriched in CTLA-4+ T cells, similar to *de novo* CHL. CLL/SLL with CHL-RT showed increased frequencies of mutations involving *XPO1, FBXW7, BIRC3, TRAF3,* and *HLA-A* versus reference CLL/SLL. No significant mutational differences were observed between CLL/SLL associated with type 1 versus type 2 CHL-RT, supporting a biological continuum. Overall, CHL-RT shares immune evasion mechanisms with *de novo* CHL and may arise from CLL/SLL with distinct genetic susceptibilities.

Key words: CLL/SLL; classic Hodgkin lymphoma; Richter's transformation; *PD-L1*/*PD-L2*, immune evasion, genetic risk, mutations

INTRODUCTION

Large cell transformation of chronic lymphocytic leukemia/small lymphocytic lymphoma (CLL/SLL), known as Richter's transformation (RT), frequently manifests as diffuse large B-cell lymphoma (DLBCL-RT) and occasionally exhibits features of classic Hodgkin lymphoma (CHL-RT). The incidence of CHL-RT is approximately 0.4% to 0.7% among CLL/SLL patients(1, 2). CHL-RT typically develops several years after the initial diagnosis of CLL/SLL, with a median interval ranging from 4.3 to 5.9 years(3, 4). Patients with CHL-RT generally experience poor outcomes, with reported median overall survival ranging from 1.1 to 3.9 years following the diagnosis of CHL (2, 5-7). However, patients treated with CHL-directed regimens have demonstrated more favorable outcomes, with median overall survival extending from 4.8 to 13.2 years (6, 8).

CHL-RT is characterized by the presence of Hodgkin/Reed-Sternberg (HRS) cells that share morphologic and immunophenotypic features with those seen in *de novo* CHL. CHL-RT can present in two distinct histologic patterns: type 1 (CLL with HRS cells), which features scattered HRS cells in a background of CLL/SLL but lacks the polymorphous inflammatory microenvironment typically seen in CHL; and type 2 (CLL with CHL), which demonstrates a full manifestation of CHL, including the characteristic inflammatory background. Previous studies have suggested that HRS cells in both type 1 and type 2 patients exhibit similar immunophenotypes and frequently demonstrate EBV-encoded RNA (EBER) positivity in 60-70% of cases(6, 9). Furthermore, HRS cells in both types of CHL-RT can be clonally related to the underlying CLL/SLL(9, 10). Importantly, type 1 may progress to type 2, and both types exhibit similar outcomes(9). In addition, type 1 patients show improved outcomes when treated with CHL-directed compared to CLL-directed therapies(6). These findings suggest that both type 1 and type 2 CHL-RT likely represent a spectrum of the same process with type 1 being an earlier stage.

While HRS cells in CHL-RT exhibit a characteristic CHL immunophenotype, as demonstrated by diagnostic markers such as CD20, PAX5, CD30, and CD15, it remains unclear whether these cells also display dysregulation of markers associated with immune evasion, a hallmark of *de novo* CHL. These include gain or amplification of *PD-L1/PD-L2* genes, overexpression of PD-L1/PD-L2 proteins, and downregulation of molecules involved in antigen presentation(11-13). In addition, HRS cells in *de novo* CHL demonstrate a distinct tumor microenvironment (TME), characterized by enrichment of cytotoxic T-lymphocyte-associated protein 4 (CTLA-4)-positive inhibitory T cells (14). Understanding these aspects may provide critical insights into the pathogenesis of CHL-RT.

Genetic factors may predispose patients with CLL/SLL to RT. DLBCL-RT is genetically characterized by mutations in several key genes, including *TP53* disruption(15-17), *CDKN2A/B* inactivation(16, 18), *NOTCH1* mutations(16, 17), and *MYC* activation(15-17), which collectively suggest a higher risk of DLBCL-RT development in CLL/SLL patients harboring these alterations. *De novo* CHL, on the other hand, is defined by mutations and copy number alterations affecting various biological pathways, such as activation of JAK-STAT and NF-κB signaling, immune evasion, and disruption of cellular homeostasis through *XPO1* mutation(19, 20). In contrast, the genetic features of CLL/SLL associated with CHL-RT have not been studied.

Leveraging a large cohort of patients with CHL-RT from 3 academic institutions, this study aims to deepen our understanding of its underlying biology. We identified a shared immune evasion phenotype in HRS cells between both types of CHL-RT and *de novo* CHL. We observed a similar TME enriched for CTLA-4-positive T cells in type 2 CHL-RT and *de novo* CHL, which was less pronounced in HRS cells from type 1 CHL-RT. Finally, we discovered distinct mutational profiles in CLL/SLL with CHL-RT, including frequent mutations in *XPO1* and *FBXW7*, histocompatibility complex gene (*HLA-A*), and genes in the NF-κB pathway (*BIRC3* and *TRAF3*).

METHODS

Patient cohort

The study was approved by the Institutional Review Boards (IRBs) and ethics committees at all participating institutions, including Memorial Sloan Kettering Cancer Center, Mayo Clinic, and the National Cancer Institute. A total of 77 CLL/SLL patients, including 27 type 1 and 50 type 2 patients, with CHL-RT were identified and collected from 3 academic institutions in the United States (**Figure 1A**). A subset of the patients included in this study has been reported previously, comprising 10 of 22 cases from the National Cancer Institute cohort and all 28 cases from the Mayo Clinic cohort(6, 9). Patient demographics, HRS cell percentages within CLL/SLL tissue, testing modalities, and clinical features are summarized in **Table 1** and **Supplementary Table 1**. A cohort of 48 *de novo* CHL cases diagnosed with 87.5% nodular sclerosis subtype at MSKCC was also included for comparison (21).

Immunohistochemistry (IHC) and in situ hybridization (ISH)

IHC and ISH staining were performed on 5-micron formalin-fixed paraffin-embedded (FFPE) tissue slides for all cases with sufficient tissue samples and HRS cells available for evaluation. Expression of PD-L1, PD-L2, MHC-I, B2M, MHC-II, and CIITA in HRS cells was assessed by IHC using a 30% positivity cut-off, as in our previous study of *de novo* CHL (21), which also served as the comparison cohort for CHL-RT.

Multiplexed immunofluorescence (mIF)

Tissue sections were stained using a six-marker multiplex immunofluorescence (mIF) assay with fluorophore-conjugated antibodies targeting the specific antigens: CD68 (Opal 480), PAX5 (Opal 520), CD86 (Opal 570), LEF1 (Opal 620), CTLA-4 (Opal 690), and PD-1 (Opal 780). Staining was performed on the Leica BOND RX automated platform (Leica Biosystems). CTLA-4 and PD-1 were included because a previous study showed that CTLA-4$^+$ T cells are enriched in the tumor microenvironment of *de novo* CHL and outnumber PD-1$^+$ cells (14).

Flow cytometric analysis

Flow cytometric studies were performed according to the protocol as described before (22). Because this was a retrospective study, flow cytometric analysis was limited to the markers in our clinically validated panel; CTLA-4 was not among them and was therefore evaluated only by mIF.

Combined CD30 immunofluorescence and *PD-L1/PD-L2* FISH analysis

Signal analysis was conducted in conjunction with tissue morphology, focusing on areas with strong CD30+ cells. Probe copy numbers were counted in up to 50 cells per case, where possible. The following criteria were used for interpreting *PD-L1/PD-L2* FISH results according to previous publication(11): amplification: *PD-L1/PD-L2/CEP9* ratio $\geq$ 3.0; gain: *PD-L1/PD-L2/CEP9* ratio > 1.0 but less than <3.0; polysomy: *PD-L1/PD-L2/CEP9* ratio ≈ 1.0 but more than two copies for each probe.

Next-generation sequencing (NGS)

The targeted NGS analysis was conducted using our laboratory-developed assay as previously described(23). Gene list is available in **Supplementary Table 2**. Only pathogenic or likely pathogenic variants were included for downstream analysis. These variants were annotated using several databases, including ClinVar(24), OncoKB(25), and COSMIC (Catalogue Of Somatic Mutations In Cancer)(26). NGS was performed on bulk CLL/SLL FFPE tissue. In addition, macrodissection was performed on samples from three patients with type 2 CHL-RT who displayed distinct areas that were enriched for either CLL/SLL or CHL, allowing for separate analysis of the CLL/SLL and CHL components. It should be noted that bulk CLL/SLL sequencing inherently included rare HRS cells, which constitute less than 5% of total cellularity.

Additional details of the materials and methods are provided in the supplement.

RESULTS

HRS cells in CHL-RT show immune evasion immunophenotype and frequent EBV positivity

Type 2 CHL-RT was predominantly of the mixed cellularity subtype. Among 43 lymph node-based cases, 30 (69.8%) were mixed cellularity, 12 (27.9%) nodular sclerosis, and 1 (2.3%) lymphocyte-depleted. We compared the immunophenotype of HRS cells between type 1 and type 2 CHL-RT, and against *de novo* CHL. HRS cells from both groups exhibited a diagnostic CHL immunophenotype, including uniform CD30 positivity, frequent CD15 expression (57.7% vs. 72%, p=0.30), dim PAX5 expression (87% vs. 81.4%, p=1.00), and frequent negativity for CD20 (72.2% vs. 78.6%, p=0.74) and CD45 (100% vs. 90.9%, p=0.55) (**Figure 1B, 1C**). EBV positivity, as detected by EBER staining, was observed in 62.5% of type 1 and 63.2% of type 2 CHL-RT cases (p=1), both significantly higher than in *de novo* CHL (17.2%, p=0.001 and p<0.001, respectively). For type 2 CHL-RT, EBV was positive in 66.7% (16/24) of mixed cellularity cases and 50.0% (3/6) of nodular sclerosis cases, whereas the single lymphocyte-depleted case was EBV-negative.

Beyond diagnostic markers, HRS cells in both CHL-RT types frequently demonstrated an immune-evasive immunophenotype, evidenced by PD-L1 expression, loss of antigen-presentation molecules, and MHC-II negativity (**Figure 2A, 2B**). Notably, PD-L1 expression was significantly lower in type 1 CHL-RT (53.3%) compared to both type 2 CHL-RT (100%, p<0.001) and *de novo* CHL (85.7%, p=0.009). MHC-I loss was more frequent in *de novo* CHL (40%) than in type 1 (18.2%) and type 2 (5.0%) CHL-RT (p=0.29 and p=0.004, respectively). Similar findings were observed in B2M, which was more frequently lost in *de novo*

CHL (64.6%) than in type 1 (6.7%) and type 2 (16.0%) CHL-RT ($p<0.001$ and $p<0.001$, respectively). In comparison, MHC-II and CIITA loss were comparable across both CHL-RT types and *de novo* CHL. PD-L2 expression was absent in type 1 and detected in only 10% of type 2 CHL-RT cases ($p=0.51$), with no significant differences observed compared to *de novo* CHL.

We further compared immune evasion phenotypes among cases with known EBV status (**Figure 2C**). Regardless of EBV status, PD-L1 expressions were less frequent in type 1 CHL-RT than in type 2 CHL-RT and *de novo* CHL. Within type 1 CHL-RT, PD-L1 expression was more common in EBV-positive than in EBV-negative cases, although the difference was not statistically significant (66.7% vs. 20.0%, $P = 0.27$). In *de novo* CHL, loss of B2M was significantly more frequent in EBV-negative than in EBV-positive cases (78.3% vs. 20.0%, $p=0.03$), and loss of MHC class I showed a similar but non-significant trend (45.5% vs. 0%, $p=0.25$). Notably, B2M loss was significantly more frequent in *de novo* CHL than in either type 1 or type 2 CHL-RT only within the EBV-negative subgroup (78.3% vs 0% vs 0%; $p=0.007$ and $p<0.001$, respectively). Given the small number of cases in each subgroup, these findings should be interpreted with caution.

HRS cells in CHL-RT show frequent gain or polysomy of *PD-L1/PD-L2*

We examined *PD-L1/PD-L2* copy number alterations in HRS cells from 12 CHL-RT cases (four cases of type 1 and eight cases of type 2) (**Figure 3A**) and compared these findings to a cohort of 84 *de novo* CHL cases diagnosed at our institution since 2021. All four type 1 and six of eight type 2 CHL-RT cases demonstrated *PD-L1/PD-L2* gain or polysomy. Of the remaining two type 2 cases, one showed *PD-L1/PD-L2* amplification and the other had a normal copy number. Compared to *de novo* CHL, HRS cells in CHL-RT showed statistically comparable frequencies of *PD-L1/PD-L2* gain or polysomy (83.3% vs. 67.9%, $p=0.34$), *PD-L1/PD-L2* amplification (8.3% vs. 26.2%, $p=0.28$), and normal *PD-L1/PD-L2* copy numbers (8.3% vs. 4.8%, $p=0.49$). *PD-L1/PD-L2* translocation, observed in only one of the 84 *de novo* CHL cases, was not detected in HRS cells associated with CHL-RT (**Figure 3B**).

Apart from two type 1 cases with *PD-L1/PD-L2* polysomy that exhibited PD-L1 negativity by IHC, all other nine cases with available IHC results showed PD-L1 positivity. These included seven cases with *PD-L1/PD-L2* polysomy, one case with *PD-L1/PD-L2* amplification, and one case with normal *PD-L1/PD-L2* copy number.

HRS cells have distinct immune microenvironment in type 1 vs 2 CHL-RT

mIF studies were performed to evaluate the TME of HRS cells in a subset of type 1 and type 2 CHL-RT, as well as in *de novo* CHL (**Figure 4A**). Using a limited panel of 6 markers, we primarily assessed the numbers of CTLA-4$^+$ and PD-1$^+$ T cells, as well as B cells, within a 75 μm radius of HRS cells (**Figure 4B**). In total, 83 HRS cells were analyzed: 33 from three type 1 CHL-RT cases (10, 10, and 13 cells per case), 33 from three type 2 CHL-RT cases (9, 10, and 14 cells per case), and 17 from two *de novo* CHL cases (8 and 9 cells per case). Compared with type I CHL-RT (median, 5 cells), HRS cells in type 2 CHL-RT (median, 24 cells; p<0.001) and *de novo* CHL (median, 18 cells; p<0.001) were surrounded by significantly more CTLA-4$^+$ T cells. PD-1$^+$ T cells were generally less numerous than CTLA-4$^+$ T cells but showed a similar pattern: they were significantly more numerous around HRS cells in type 2 CHL-RT than in type I CHL-RT (median, 6 vs 2 cells; p=0.010), with a similar but non-significant trend in *de novo* CHL (median, 5 cells; p=0.061). Finally, as expected, B cells (likely CLL/SLL cells in CHL-RT) were significantly more abundant around HRS cells in both type 1 (median, 74 cells; p<0.001) and type 2 CHL-RT (median, 41 cells; p<0.001) than in *de novo* CHL (median, 7 cells), whereas the difference between type 1 and 2 CHL-RT was not significant.

We further compared T cell composition by flow cytometry between CHL-RT and a cohort of *de novo* CHL (**Figure 4C**). The two groups demonstrated similar CD4:CD8 ratios within the T cell compartment (median, 2.8 vs 4.0; *p*=0.196). In contrast, CHL-RT cases exhibited lower proportions of CD25$^+$ T cells (median, 6.1% vs 14.8%; *p*=0.041) and higher proportions of PD-1$^+$ T cells (median, 8.9% vs 0.9%; *p*=0.043) within the CD4$^+$ T cell compartment compared with *de novo* CHL.

CLL/SLL with CHL-RT show distinct genetic profiles

NGS studies were conducted on bulk FFPE tissue of 37 CLL/SLL samples with CHL-RT (HRS cells <5%), including 18 samples with type 1 and 19 samples with type 2 CHL-RT. Genes recurrently mutated in more than one sample were selected for further comparison **(Figure 5A**). The most frequently mutated genes in the combined cohort of type 1 and type 2 CHL-RT included *XPO1* (16.2%, 6/37), *FBXW7* (16.2%, 6/37), *BIRC3* (13.5%, 5/37), *SF3B1* (10.8%, 4/37), *NOTCH1* (10.8%, 4/37), and *TP53* (10.8%, 4/37), among others. Mutations in several genes were more frequently observed in type 1 CLL/SLL, including *XPO1* (27.8% vs 5.3%), *NOTCH1* (16.7% vs 5.3%), *BRAF* (16.7% vs 0%), *KRAS* (11.1% vs 0%), *HLA-A* (11.1%

vs 0%), *EGR2* (11.1% vs 0%), *SETD2* (11.1% vs 0%), and *MED12* (11.1% vs 0%), while other genes were more frequently mutated in type 2 CLL/SLL, including *TP53* (5.6% vs 15.8%) and *CHD2* (0% vs 10.5%); however, these differences did not reach statistical significance (**Figure 5B**). Variant allele frequencies (VAFs) for all mutations were greater than 2%, with the majority exceeding 5% (**Figure 5C)**, suggesting that these alterations were unlikely to be derived from HRS cells.

XPO1 and *FBXW7,* two genes involved in maintaining protein homeostasis, were among the most frequent alterations (10 cases in total, 27%). All *XPO1* mutations were missense mutations at the hotspot locus p.E571. Mutations involving the epigenetic regulators (*KMT2D*/*CHD2*/*MED12*, 7 cases in total, 18.9%) or the canonical NF-κB pathway (*BIRC3*/*TRAF3*, 6 cases in total, 16.2%) were also frequently detected. Other involved pathways include Notch signaling (*NOTCH1/2*, 5 cases in total, 13.5%), RNA splicing (*SF3B1*, 4 cases, 10.8%), MAPK pathway signaling (*BRAF/KRAS*, 4 cases, 10.8%). Of note, three of the four patients with *TP53* mutations belonged to the type 2 CHL-RT group, and an *ATM* mutation was only detected in one type 2 CHL-RT case.

When comparing the combined CHL-RT cohort to a reference CLL/SLL cohort (n=2743), comprising cases from our in-house clinical sequencing database and data from three additional studies available through cBioPortal(27-29), several genes were found to be significantly more frequently mutated in CLL/SLL with CHL-RT (**Figure 5D**). These included *XPO1* (16.2% vs. 3.8%, p=0.002), *FBXW7* (16.2% vs. 3.4%, p=0.001), *BIRC3* (13.5% vs. 3.2%, p=0.006), and *HLA-A* (5.4% vs. 0.05%, p=0.001). *TRAF3* was also more commonly mutated in CLL/SLL with CHL-RT despite not reaching statistical significance (5.4% vs 1.0%, p=0.05).

We also compared the frequencies of common cytogenetic abnormalities between type 1 (n=12) and type 2 (n=27) CLL/SLL with CHL-RT and a reference CLL/SLL cohort (n=2,028) compiled from six published studies (30-35) (**Figure 5E**). Overall, the frequencies of del(17p) and del(13q) in CLL/SLL with CHL-RT were comparable to those of the reference cohort. In contrast, del(11q) and trisomy 12 were each present in 50% (6/12) of type 1 CLL/SLL cases, compared with 23.1% (6/26) and 22.2 (6/27), respectively, in type 2 CLL/SLL, and 13.6% (276/2,028) and 23.5% (476/2,028), respectively, in the reference cohort. However, these differences were statistically significant only between type 1 CLL/SLL and the reference cohort (p = 0.003 and p = 0.042, respectively). IGHV mutational status was available for 15 cases of CLL/SLL with

CHL-RT. Unmutated IGHV was identified in 75% (3/4) of type 1 and 63.6% (7/11) of type 2 cases (66.7% overall, 10/15), a higher proportion than the approximately 40% reported in the general CLL/SLL population(36, 37).

NGS was also performed on bulk FFPE tissue from three patients with type 2 CHL-RT in whom the samples showed CHL with a high density of HRS cells and no morphologic or immunophenotypic evidence of the previously diagnosed CLL/SLL. The first patient (case #28), with approximately 10% HRS cells, harbored an *HLA-A* mutation (VAF 11.2%). The second patient (case #59), with 20–30% HRS cells, harbored an *SRSF2* mutation (VAF 10.7%). The third patient (case #68), with 10–20% HRS cells, had no pathogenic or likely pathogenic mutations detected.

Comparison of mutational profiles in paired CHL and CLL/SLL

We conducted paired NGS on macrodissected areas enriched for either CLL/SLL or CHL from the same specimens in 3 type 2 CHL-RT patients, enabling us to analyze the mutational spectrum and clonal relationships between the two neoplastic processes (**Figure 6**). The proportion of CLL/SLL and HRS cells in the macrodissected areas was estimated by PAX5 (focusing on positive small cells) and CD30 IHCs, respectively. In the first patient (case #63), distinct mutations were identified in the CLL/SLL- and CHL-enriched areas, with no shared mutations observed. Given the neoplastic burden in each area, it is most likely that there were no shared mutations between the CLL/SLL and HRS cells in this case. The second patient (case #30) exhibited multiple shared mutations with similar VAFs between the CLL/SLL- and CHL-enriched areas, indicating a clonal relatedness. Considering the relative abundance of HRS cells, it is favored that these mutations indeed originate from HRS cells, rather than background CLL/SLL. In the third patient (case #71), no mutation was detected in both the CLL/SLL and the CHL-enriched area; however, as HRS cells constituted only 3-5% of the macrodissected CHL area, the possibility of false negativity due to low tumor content cannot be excluded.

Patients with type 1 and type 2 CHL-RT show similar demographics and clinical outcomes

Patients with type 1 and type 2 CHL-RT shared similar demographic characteristics, including a male predominance in both groups (77.8% vs. 72%, respectively; p=0.79) and comparable median ages at CHL-RT diagnosis (71 vs. 70.5 years, respectively; p=0.14) (**Figure 7A**). The interval between CLL/SLL and CHL diagnoses was likewise similar, with median times of 5.3 years for type 1 and 3.5 years for type 2

CHL-RT (p=0.16) (**Figure 7B**). Four patients had both type 1 and type 2 CHL-RT, diagnosed in separate specimens. In two patients, the two subtypes were identified concurrently at different sites, whereas the other two were initially diagnosed with type 1 CHL-RT and developed type 2 CHL-RT 6 months and 2 years later, respectively.

Data on prior CLL/SLL treatment were available for 10 type 1 and 21 type 2 CHL-RT patients. Both groups had received a median of two prior lines of therapy, with comparable exposure (type 1 vs type 2) to immunotherapy-based regimens (80.0% vs. 61.9%), Bruton tyrosine kinase inhibitors (30.0% vs. 23.8%), or DLBCL-directed therapy (10.0% vs. 9.5%). All type 1 patients had received prior CLL/SLL therapies, whereas 2 patients (9.5%) with type 2 CHL-RT had been managed with active surveillance alone. Data on CHL-RT treatment were available for 13 type 1 and 26 type 2 patients. Most patients received CHL-directed therapy (61.5% vs. 88.5%), while DLBCL-directed therapy was uncommon (15.4% vs. 11.5%). CLL/SLL-directed therapy was given only to patients with type 1 CHL-RT (23.1% vs. 0%). Detailed treatment histories are provided in the Supplementary Material.

Overall survival (OS) did not differ significantly between the two subtypes, when measured from CLL/SLL diagnosis (median OS, 10.5 vs 15.0 years for type 1 vs type 2, p=0.95; **Figure 7C**) or from CHL-RT diagnosis (median OS, 2.7 vs 5.3 years, p=0.12; **Figure 7D**), although OS from CHL-RT diagnosis tended to be shorted in type 1 CHL-RT. Among patients with available CHL-RT treatment data, OS measured from CLL/SLL diagnosis remained comparable between the groups (median OS, 10.5 vs 15.0 years, p=0.97; **Figure 7E**), whereas OS measured from CHL-RT diagnosis was significantly shorter in type 1 CHL-RT (median OS, 2.7 vs 5.4 years, p=0.04; **Figure 7F**).

In subgroup analysis of type I CHL-RT, patients who received CHL-directed therapy had significantly longer OS than those who received other regimens (CLL/SLL- or DLBCL-directed therapy) (median OS, 5.5 vs 0.6 years, p=0.002, **Figure 7G**). Notably, among patients who received CHL-directed therapy, OS was comparable between type 1 and type 2 CHL-RT (median OS, 5.5 vs. 5.4 years, p=0.63, **Figure 7G**).

DISCUSSION

We provide novel evidence that HRS cells in CHL-RT and *de novo* CHL share a common immune evasion phenotype, including frequent *PD-L1/PD-L2* gain/amplification, establishing for the first time a shared biological and genetic basis between these two conditions.

A key distinction, however, emerged in the tumor microenvironment. PD-L1 expression on HRS cells was significantly lower in type 1 CHL-RT as compared to both type 2 CHL-RT and *de novo* CHL. This difference was most pronounced among cases with EBV-negative HRS cells, consistent with the established role of EBV infection in promoting PD-L1 expression(38). Using mIF, we demonstrated that this difference reflects a fundamentally less immunosuppressive TME in type 1 CHL-RT, with lower number of both CTLA-4$^+$ and PD-1$^+$ T cells. In contrast, these immunosuppressive T cell populations were comparably dense in type 2 CHL-RT and *de novo* CHL. Collectively, these findings indicate that type 2 CHL-RT fully recapitulates the immunosuppressive microenvironment of *de novo* CHL, while type 1 CHL-RT represents an earlier stage of incomplete microenvironmental reprogramming. This interpretation is further supported by the direct observation (including our cohort) of patients who demonstrated type 1 histology on initial biopsy with subsequent progression to type 2 CHL-RT (6, 9), suggesting a chronological evolution from type 1 to type 2. This shared suppressive TME provides a biological rationale for exploring immune checkpoint inhibitors in CHL-RT, particularly in type 2 disease, where the microenvironment most closely mirrors that of *de novo* CHL, a setting in which PD-1 blockade has demonstrated established clinical efficacy(39). The less pronounced but present immune-evasive phenotype in type 1 CHL-RT similarly warrants investigation into whether checkpoint inhibition may have a role in this subtype.

In contrast, loss of MHC-I and B2M expression by HRS cells was less frequent in CHL-RT than in *de novo* CHL. This suggests that CHL-RT may rely less on impaired antigen presentation to evade immune surveillance. One possible explanation is that the immunosuppressive milieu associated with the underlying CLL/SLL already provides an alternative route of immune escape, reducing the selective pressure to lose MHC-I expression. Consistent with previous studies(40, 41), we also found that loss of B2M, and to a lesser extend MHC-I, was more frequent in in EBV-negative than in EBV-positive *de novo* CHL.

Our NGS analysis reveals a distinct mutational landscape that identifies potential genetic risk factors for CHL-RT. Most notably, *XPO1* hotspot mutations (p.E571) were identified in 16.2% of CLL/SLL with CHL-RT, comparable to the 13.1% frequency reported in flow sorted HRS cells from *de novo* CHL(19, 20),

suggesting that *XPO1* mutations potentially represent a shared genetic risk factor for Hodgkin lymphomagenesis in both disease contexts. This finding is therapeutically relevant, as XPO1 is targetable by the small-molecule inhibitor selinexor (KPT-330), which has demonstrated preclinical efficacy in lymphoma and leukemia models and is now in clinical use. Interestingly, *XPO1* mutations were more frequently observed in CLL/SLL cases with type 1 CHL-RT (27.8%) compared with those with type 2 CHL-RT (5.3%); however, this difference did not reach statistical significance ($p = 0.09$), likely due to the relatively small sample size. It remains unclear whether CLL/SLL cases associated with type 1 versus type 2 CHL-RT harbor fundamentally distinct mutational profiles, or whether differences in HRS cell biology between the two subtypes account for the observed variability. Larger-scale studies with improved single cell sequencing technology will be required to validate these observations and to further elucidate the biological differences between these entities. Beyond *XPO1*, enrichment of mutations in *FBXW7* (regulating c-Myc/Notch turnover), NF-κB pathway genes (*BIRC3*, *TRAF3*), and immune-related genes (*HLA-A*) suggest that enhanced NF-κB signaling and acquisition of immune evasion, hallmarks of *de novo* CHL, may contribute to CHL-RT predisposition.

Despite these enrichments, the overall genetic profile of CLL/SLL with CHL-RT remains broadly similar to conventional CLL/SLL. Highly recurrent *de novo* CHL mutations (*B2M*, *SOCS1*, *STAT6*, *TNFAIP3*, *ITPKB*) were not detected, and no individual gene exceeded a 20% mutation frequency, suggesting that CHL-RT risk reflects complex polygenic interactions rather than single driver events. Notably, the genetic risk profile of CHL-RT appears distinct from DLBCL-RT, which is characterized by *TP53* disruption(15-17), *CDKN2A/B* inactivation(16, 18), *NOTCH1* mutations(16, 17), and *MYC* activation(15-17), none of which were enriched in our cohort (copy number data were unavailable to assess *CDKN2A/B*). This distinction underscores that CHL-RT and DLBCL-RT, while both arising from CLL/SLL, are driven by fundamentally different genetic programs.

This study has several limitations. The most significant is the lack of genetic data from isolated HRS cells. Without these data, we could not identify HRS-specific mutations or compare clonally related with clonally unrelated CHL-RT. Similarly, apart from *PD-L1/PD-L2*, copy number alteration data from isolated HRS cells were not available, which limits direct comparison with *de novo* CHL. Our genomic analysis was therefore focused on the CLL/SLL component. Although NGS was performed on bulk tissue, most recurrent mutations had VAFs greater above 5%, suggesting that these alterations most likely arose in the CLL/SLL population. Whether they are also present in the HRS cells could not be determined. Future studies using

spatial single-cell sequencing of HRS cells will be needed to define the HRS-specific genomic alterations in CHL-RT and to determine whether mutations identified in the CLL/SLL component are shared by HRS cells. In addition, the small number of cases in some subgroups, particularly in the mIF and EBV-stratified analyses, limited statistical power. Finally, this retrospective study included cases from multiple institutions diagnosed over a long period (1995-2022) and treated with heterogeneous regimens, which precludes definitive conclusions about survival outcomes.

In summary, this study provides the first integrated immunophenotypic and genomic characterization of CHL-RT, establishing biological links to *de novo* CHL. These findings lay a foundation for future mechanistic and therapeutic investigations of this rare and biologically distinct form of Richter transformation.

REFERENCES

1. Tsimberidou AM, O'Brien S, Kantarjian HM, et al. Hodgkin transformation of chronic lymphocytic leukemia: the M. D. Anderson Cancer Center experience. Cancer. 2006;107(6):1294-1302.

2. Parikh SA, Habermann TM, Chaffee KG, et al. Hodgkin transformation of chronic lymphocytic leukemia: Incidence, outcomes, and comparison to de novo Hodgkin lymphoma. Am J Hematol. 2015;90(4):334-338.

3. Bockorny B, Codreanu I, Dasanu CA. Hodgkin lymphoma as Richter transformation in chronic lymphocytic leukaemia: a retrospective analysis of world literature. Br J Haematol. 2012;156(1):50-66.

4. Tadmor T, Shvidel L, Goldschmidt N, et al. Hodgkin's variant of Richter transformation in chronic lymphocytic leukemia; a retrospective study from the Israeli CLL study group. Anticancer Res. 2014;34(2):785-790.

5. Zhu K, Jamroz A, Huang S, et al. Outcomes of Hodgkin variant Richter transformation in chronic lymphocytic leukaemia and small lymphocytic lymphoma in British Columbia. Br J Haematol. 2022;198(4):684-692.

6. King RL, Gupta A, Kurtin PJ, et al. Chronic lymphocytic leukemia (CLL) with Reed-Sternberg-like cells vs Classic Hodgkin lymphoma transformation of CLL: does this distinction matter? Blood Cancer J. 2022;12(1):18.

7. Drozd-Sokolowska J, Zaucha JM, Zoltak T, et al. Hodgkin lymphoma transformation of chronic lymphocytic leukemia-A real life data from the Polish Lymphoma Research Group. Hematol Oncol. 2019;37(4):383-391.

8. Stephens DM, Boucher K, Kander E, et al. Hodgkin lymphoma arising in patients with chronic lymphocytic leukemia: outcomes from a large multi-center collaboration. Haematologica. 2021;106(11):2845-2852.

9. Xiao W, Chen WW, Sorbara L, et al. Hodgkin lymphoma variant of Richter transformation: morphology, Epstein-Barr virus status, clonality, and survival analysis-with comparison to Hodgkin-like lesion. Hum Pathol. 2016;55:108-116.

10. Ohno T, Smir BN, Weisenburger DD, Gascoyne RD, Hinrichs SD, Chan WC. Origin of the Hodgkin/Reed-Sternberg cells in chronic lymphocytic leukemia with "Hodgkin's transformation". Blood. 1998;91(5):1757-1761.

11. Roemer MG, Advani RH, Ligon AH, et al. PD-L1 and PD-L2 Genetic Alterations Define Classical Hodgkin Lymphoma and Predict Outcome. J Clin Oncol. 2016;34(23):2690-2697.

12. Liu WR, Shipp MA. Signaling pathways and immune evasion mechanisms in classical Hodgkin lymphoma. Blood. 2017;130(21):2265-2270.

13. Van den Berg A, Visser L, Eberwine J, Dadvand L, Poppema S. Frequent lack of translation of antigen presentation-associated molecules MHC class I, CD1a and Beta(2)-microglobulin in Reed-Sternberg cells. Int J Cancer. 2000;86(4):548-552.

14. Patel SS, Weirather JL, Lipschitz M, et al. The microenvironmental niche in classic Hodgkin lymphoma is enriched for CTLA-4-positive T cells that are PD-1-negative. Blood. 2019;134(23):2059-2069.

15. Rossi D, Spina V, Deambrogi C, et al. The genetics of Richter syndrome reveals disease heterogeneity and predicts survival after transformation. Blood. 2011;117(12):3391-3401.

16. Petrackova A, Turcsanyi P, Papajik T, Kriegova E. Revisiting Richter transformation in the era of novel CLL agents. Blood Rev. 2021;49:100824.

17. Tadmor T, Levy I. Richter transformation in chronic lymphocytic leukemia: update in the era of novel agents. Cancers (Basel). 2021;13(20):5141.

18. Fabbri G, Khiabanian H, Holmes AB, et al. Genetic lesions associated with chronic lymphocytic leukemia transformation to Richter syndrome. J Exp Med. 2013;210(11):2273-2288.

19. Maura F, Ziccheddu B, Xiang JZ, et al. Molecular evolution of classic Hodgkin lymphoma revealed through whole-genome sequencing of Hodgkin and Reed Sternberg cells. Blood Cancer Discov. 2023;4(3):208-227.

20. Wienand K, Chapuy B, Stewart C, et al. Genomic analyses of flow-sorted Hodgkin Reed-Sternberg cells reveal complementary mechanisms of immune evasion. Blood Adv. 2019;3(23):4065-4080.

21. Pourmaleki M, Jones CJ, Mellinghoff SD, et al. Multiplexed spatial profiling of Hodgkin Reed-Sternberg cell neighborhoods in classic Hodgkin lymphoma. Clin Cancer Res. 2024;30(17):3881-3893.

22. Chan A, Gao Q, Roshal M. 19-color, 21-antigen single tube for efficient evaluation of B- and T-cell neoplasms. Curr Protoc. 2023;3(9):e884.

23. Ptashkin RN, Ewalt MD, Jayakumaran G, et al. Enhanced clinical assessment of hematologic malignancies through routine paired tumor and normal sequencing. Nat Commun. 2023;14(1):6895.

24. Landrum MJ, Lee JM, Riley GR, et al. ClinVar: public archive of relationships among sequence variation and human phenotype. Nucleic Acids Res. 2014;42(Database issue):D980-985.

25. Chakravarty D, Gao J, Phillips SM, et al. OncoKB: a precision oncology knowledge base. JCO Precis Oncol. 2017;2017:PO.17.00011.

26. Forbes SA, Beare D, Gunasekaran P, et al. COSMIC: exploring the world's knowledge of somatic mutations in human cancer. Nucleic Acids Res. 2015;43(Database issue):D805-811.

27. Puente XS, Bea S, Valdes-Mas R, et al. Non-coding recurrent mutations in chronic lymphocytic leukaemia. Nature. 2015;526(7574):519-524.

28. Landau DA, Carter SL, Stojanov P, et al. Evolution and impact of subclonal mutations in chronic lymphocytic leukemia. Cell. 2013;152(4):714-726.

29. Quesada V, Conde L, Villamor N, et al. Exome sequencing identifies recurrent mutations of the splicing factor SF3B1 gene in chronic lymphocytic leukemia. Nat Genet. 2011;44(1):47-52.

30. Dohner H, Stilgenbauer S, Benner A, et al. Genomic aberrations and survival in chronic lymphocytic leukemia. N Engl J Med. 2000;343(26):1910-1916.

31. Reddy KS. Chronic lymphocytic leukaemia profiled for prognosis using a fluorescence in situ hybridisation panel. Br J Haematol. 2006;132(6):705-722.

32. Qiu HX, Xu W, Cao XS, et al. Cytogenetic characterisation in Chinese patients with chronic lymphocytic leukemia: a prospective, multicenter study on 143 cases analysed with interphase fluorescence in situ hybridisation. Leuk Lymphoma. 2008;49(10):1887-1892.

33. Lai YY, Huang XJ. Cytogenetic characteristics of B cell chronic lymphocytic leukemia in 275 Chinese patients by fluorescence in situ hybridization: a multicenter study. Chin Med J (Engl). 2011;124(16):2417-2422.

34. Amare PS, Gadage V, Jain H, et al. Clinico-pathological impact of cytogenetic subgroups in B-cell chronic lymphocytic leukemia: experience from India. Indian J Cancer. 2013;50(3):261-267.

35. Harris RA, Stevens JM, Pickering DL, et al. Frequency, variations, and prognostic implications of chromosome 14q32 deletions in chronic lymphocytic leukemia. Leuk Res. 2021;110:106665.

36. Nabki J, Al Deeban B, Sium AM, et al. Immunoglobulin light chain mutational status refines IGHV prognostic value in identifying chronic lymphocytic leukemia patients with early treatment requirement. Leukemia. 2025;39(3):643-649.

37. Huet S, Bouvard A, Ferrant E, et al. Impact of using leader primers for IGHV mutational status assessment in chronic lymphocytic leukemia. Leukemia. 2020;34(8):2257-2259.

38. Green MR, Rodig S, Juszczynski P, et al. Constitutive AP-1 activity and EBV infection induce PD-L1 in Hodgkin lymphomas and posttransplant lymphoproliferative disorders: implications for targeted therapy. Clin Cancer Res. 2012;18(6):1611-1618.

39. Herrera AF, LeBlanc M, Castellino SM, et al. Nivolumab+AVD in advanced-stage classic Hodgkin's lymphoma. N Engl J Med. 2024;391(15):1379-1389.

40. Murray PG, Constandinou CM, Crocker J, Young LS, Ambinder RF. Analysis of major histocompatibility complex class I, TAP expression, and LMP2 epitope sequence in Epstein-Barr virus-positive Hodgkin's disease. Blood. 1998;92(7):2477-2483.

41. Oudejans JJ, Jiwa NM, Kummer JA, et al. Analysis of major histocompatibility complex class I expression on Reed-Sternberg cells in relation to the cytotoxic T-cell response in Epstein-Barr virus-positive and -negative Hodgkin's disease. Blood. 1996;87(9):3844-3851.

Table 1: Summary of patient cohort

		CHL-RT type	
		Type 1 (n=27)	**Type 2 (n=50)**
Sex, male (%)		21 (77.8%)	36 (72%)
Age at CLL/SLL diagnosis, median (range)		63 (45 to 86)	64 (37 to 87)
Age at CHL-RT diagnosis, median (range)		71 (45 to 90)	70.5 (38 to 88)
HRS cells % in CLL/SLL tissue, number (%)	≤ 5%	26 (96.3%)	37 (74%)
	5-10%	0	6 (12%)
	≥ 10%	1 (3.7%)	7 (14%)
Years from CLL/SLL to CHL-RT diagnosis, median (range)		5.5 (0 to 35.0)	3.5 (0 to 22.1)
IHC for immune markers tested, number (%)		18 (66.7%)	31 (60.0%)
Bulk NGS for CLL/SLL tested, number (%)		18 (66.7%)	20 (40.0%)
FISH for *PD-L1/PD-L2* tested, number (%)		4 (14.8%)	8 (16.0%)
Multiplex IF tested, number (%)		3 (11.1%)	3 (6.0%)

FIGURE LEGENDS

Figure 1. Cohort composition and baseline immunophenotype of Hodgkin/Reed-Sternberg (HRS) cells in classical Hodgkin lymphoma variant Richter transformation (CHL-RT).

(A) Summary of case contributions from three institutions and the number of cases included in downstream immunophenotypic, tumor microenvironment, and molecular genetic analyses (MSK, Memorial Sloan Kettering Cancer Center; Mayo, Mayo Clinic Rochester; NIH, National Institutes of Health/National Cancer Institute).

(B) Representative histopathologic features of type 1 and type 2 CHL-RT. Type 1 CHL-RT demonstrate scattered HRS cells (highlighted by CD30 IHC) within a chronic lymphocytic leukemia/small lymphocytic lymphoma (CLL/SLL) background (highlighted by PAX5 IHC), whereas type 2 CHL-RT shows HRS cells embedded in a characteristic polymorphous inflammatory background.

(C) Comparison of baseline immunophenotypic features and Epstein-Barr virus (EBV) status of HRS cells, assessed by EBER in situ hybridization, between type 1 and type 2 CHL-RT.

Figure 2. Immune evasion phenotype in CHL-RT compared with *de novo* CHL.

(A) Representative immunohistochemical images illustrating immune evasion marker expression patterns in CHL-RT HRS cells (positive examples shown on the left, negative examples on the right), including PD-L1, PD-L2, MHC-I, B2M, MHC-II, and CIITA. Representative HRS cells are indicated by black arrows.

(B) Comparison of immune evasion marker expression, along with EBV status by EBER in situ hybridization, in HRS cells from type 1 CHL-RT, type 2 CHL-RT, and *de novo* CHL. *, $p < 0.05$.

(C) Comparison of immune evasion marker expression in HRS cells from type 1 CHL-RT, type 2 CHL-RT, and *de novo* CHL by their EBV status. *, $p < 0.05$.

Figure 3. *PD-L1/PD-L2* copy number alterations in CHL-RT compared with *de novo* CHL.

(A) Assessment of *PD-L1/PD-L2* copy number alterations (CNAs) in CHL-RT using combined CD30 immunofluorescence (IF) and *PD-L1/PD-L2* fluorescence in situ hybridization (FISH) with CEP9 (centromeric probe for chromosome 9) as a control. Representative images demonstrate patterns classified as normal, polysomy, gain, and amplification of *PD-L1/PD-L2* (definitions provided in Materials and Methods). For each field, paired images are shown, with the left panel displaying *PD-L1*, *PD-L2*, and CD30 signals, and the right panel displaying *PD-L1*, *PD-L2*, and CEP9 signals.

(B) Comparison of *PD-L1/PD-L2* CNAs in HRS cells from CHL-RT versus *de novo* CHL.

Figure 4. Spatial immune microenvironment of HRS cells in type 1 and type 2 CHL-RT and *de novo* CHL.

(A) Representative multiplex immunofluorescence (mIF) images depicting the cellular neighborhood surrounding HRS cells in type 1 CHL-RT, type 2 CHL-RT, and *de novo* CHL. The six-marker panel

includes CD68, PAX5, CD86, LEF1, CTLA-4, and PD-1, with DAPI nuclear counterstain. HRS cells are identified based on morphology and co-expression of PAX5 and CD86 (highlighted by white arrows).

(B) Quantitative spatial analysis of CTLA-4$^+$ cells, PD-1$^+$ cells, and B-cell populations within a 75-μm radius of individual HRS cells. A total of 33 HRS cells from three type 1 cases, 33 HRS cells from three type 2 cases, and 17 HRS cells from two *de novo* CHL cases were analyzed. Black bars indicate group medians. **, $p < 0.01$; ***, $p < 0.001$; ****, $p < 0.0001$.

(C) Flow cytometric comparison of T-cell subsets between CHL-RT and *de novo* CHL, including CD4:CD8 ratio, proportion of CD25$^+$ T cells, and proportion of PD-1$^+$ cells within the CD4$^+$ T-cell compartment. Black bars indicate group medians. *, $p < 0.05$.

Figure 5. Distinct mutational landscape of CLL/SLL associated with CHL-RT.

(A) Oncoplot summarizing pathogenic and likely pathogenic variants identified by targeted next-generation sequencing (MSK-IMPACT-Heme) in bulk CLL/SLL samples from patients with CHL-RT. Genes recurrently mutated in two or more samples are shown. CHL-RT subtype (type 1 vs type 2) and de-identified patient IDs are indicated at the bottom of the plot.

(B) Comparison of mutation frequencies between type 1 and type 2 CHL-RT-associated CLL/SLL for selected recurrently mutated genes. Differences did not reach statistical significance.

(C) Comparison of variant allele frequencies between type 1 and type 2 CHL-RT-associated CLL/SLL for selected recurrently mutated genes. Black bars indicate group median.

(D) Comparison of mutation frequencies in CHL-RT-associated CLL/SLL versus a reference CLL/SLL cohort derived from institutional databases and published cohorts. *, $p < 0.05$.

(E) Comparison of common cytogenetic abnormalities among type 1 and type 2 CHL-RT-associated CLL/SLL and a reference CLL/SLL cohort. *, $p < 0.05$.

Figure 6. Paired sequencing of macrodissected CLL/SLL- and CHL-enriched areas in type 2 CHL-RT.

Targeted next-generation sequencing (NGS) results from paired macrodissected regions enriched for CLL/SLL versus CHL from the same specimens in three patients with type 2 CHL-RT. Estimated neoplastic burden in each region was assessed by PAX5 and CD30 IHCs. Detected mutations in paired regions are displayed to infer clonal relatedness between the CLL/SLL and CHL components.

Figure 7. Clinical characteristics and outcomes of type 1 vs type 2 CHL-RT.

(A) Age at CHL-RT diagnosis for type 1 vs type 2 patients. Black bars indicate group median. ns, statistically not significant.

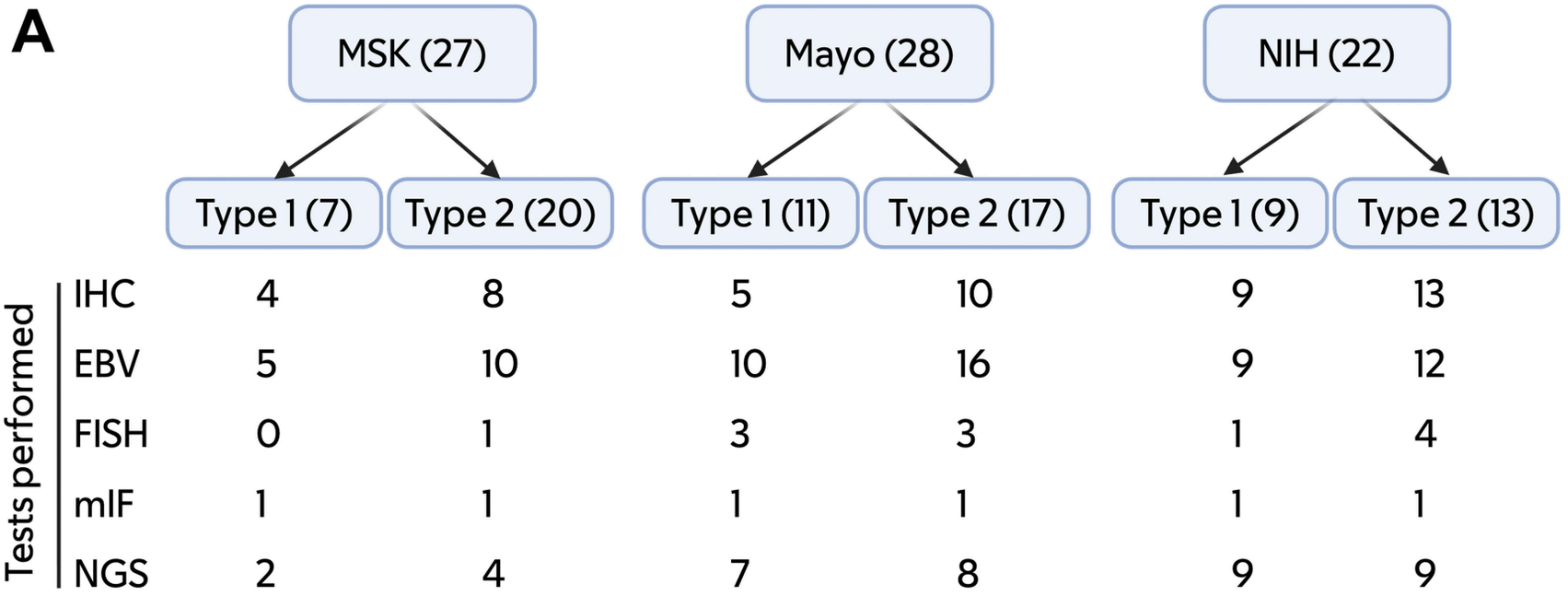
(B) Interval from CLL/SLL to CHL-RT diagnosis in type 1 vs type 2 CHL-RT. Black bars indicate group median. ns, statistically not significant.

(C-D) Kaplan–Meier overall survival (OS) analysis for all patients with type 1 versus type 2 CHL-RT, calculated from either the time of CLL/SLL diagnosis (C) or the time of CHL-RT diagnosis (D).

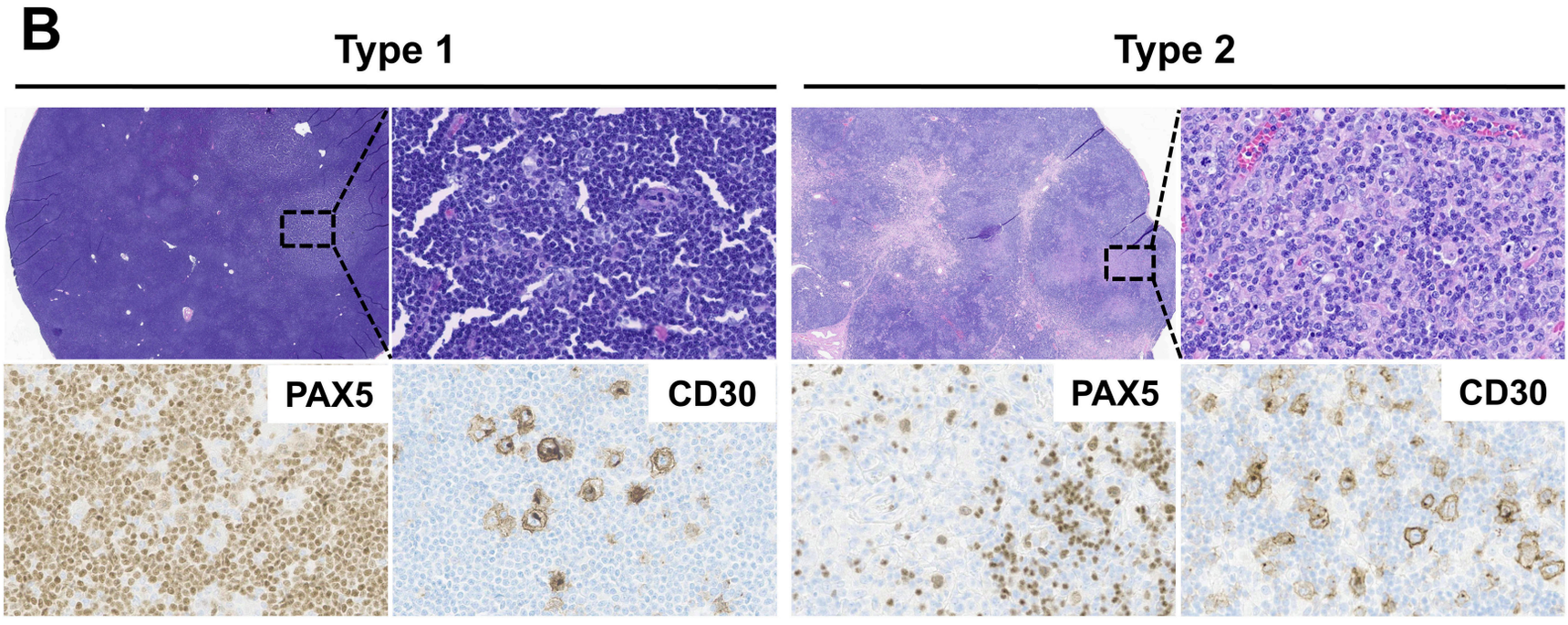
(E-F) Kaplan-Meier OS analysis for patients with type 1 versus type 2 CHL-RT with available treatment information for CHL-RT, calculated from either the time of CLL/SLL diagnosis (E) or the time of CHL-RT diagnosis (F).

(G) Kaplan–Meier OS analysis from the time of CHL-RT diagnosis, stratified by treatment regimen (CHL-directed vs. other therapies) in type 1 and type 2 CHL-RT. **, $p < 0.01$.

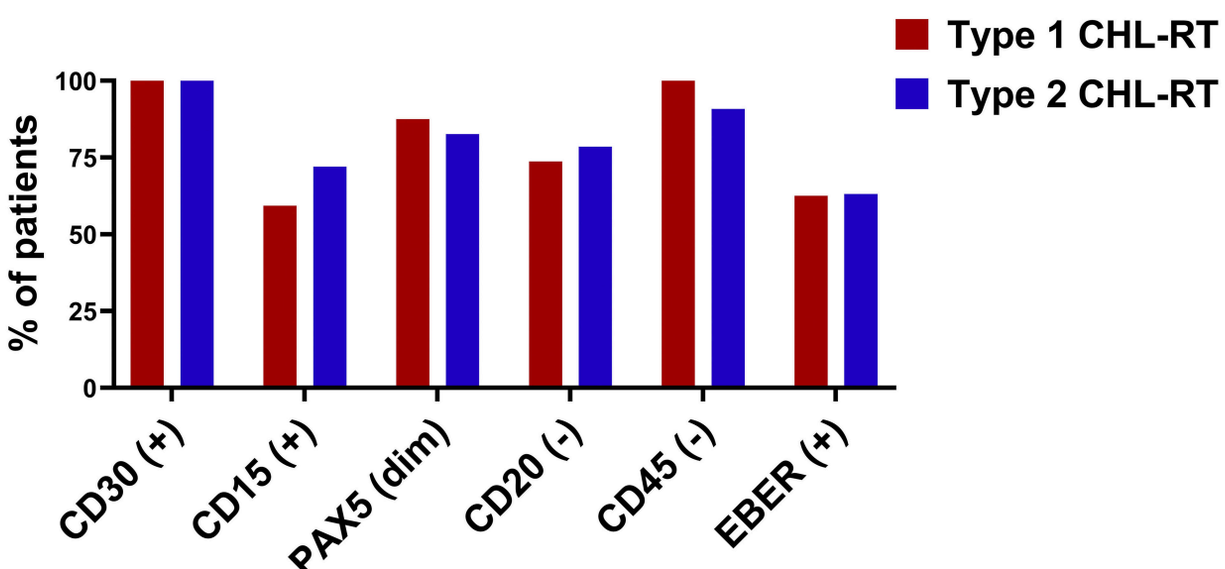
A

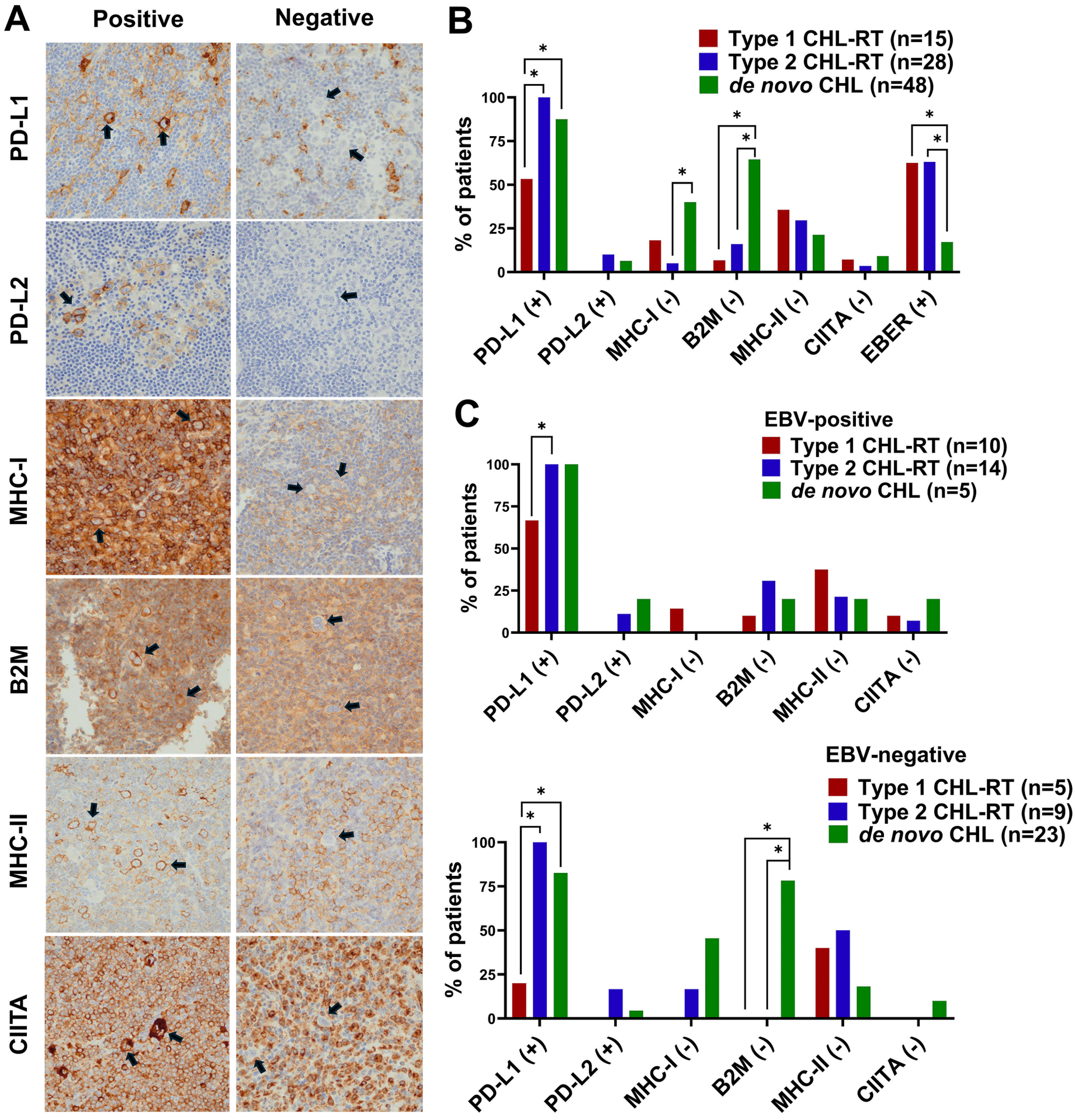

MSK (27)
Mayo (28)
NIH (22)
Type 1 (7)
Type 2 (20)
Type 1 (11)
Type 2 (17)
Type 1 (9)
Type 2 (13)
Tests performed
IHC 4 8 5 10 9 13
EBV 5 10 10 16 9 12
FISH 0 1 3 3 1 4
mIF 1 1 1 1 1 1
NGS 2 4 7 8 9 9

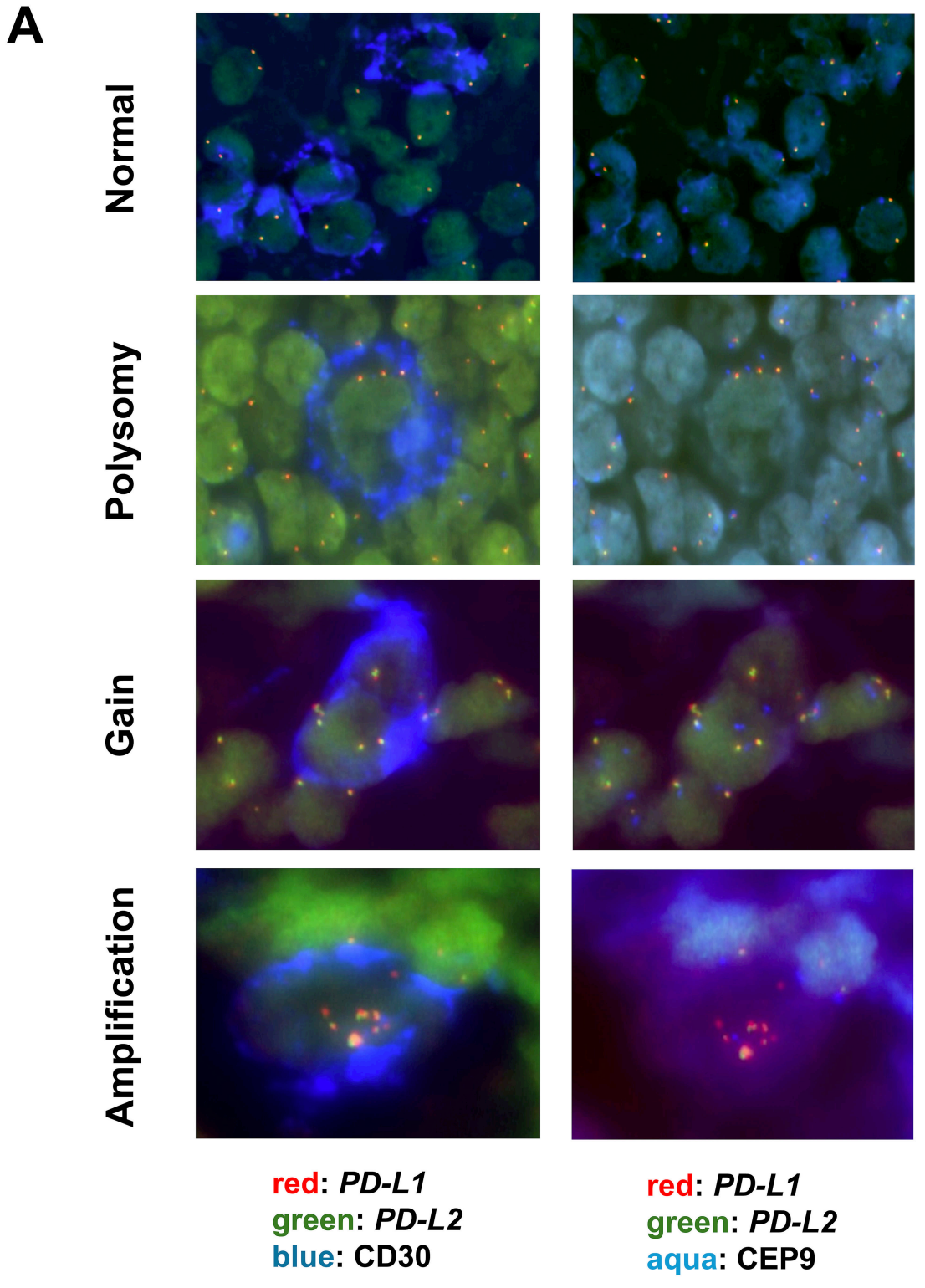
B

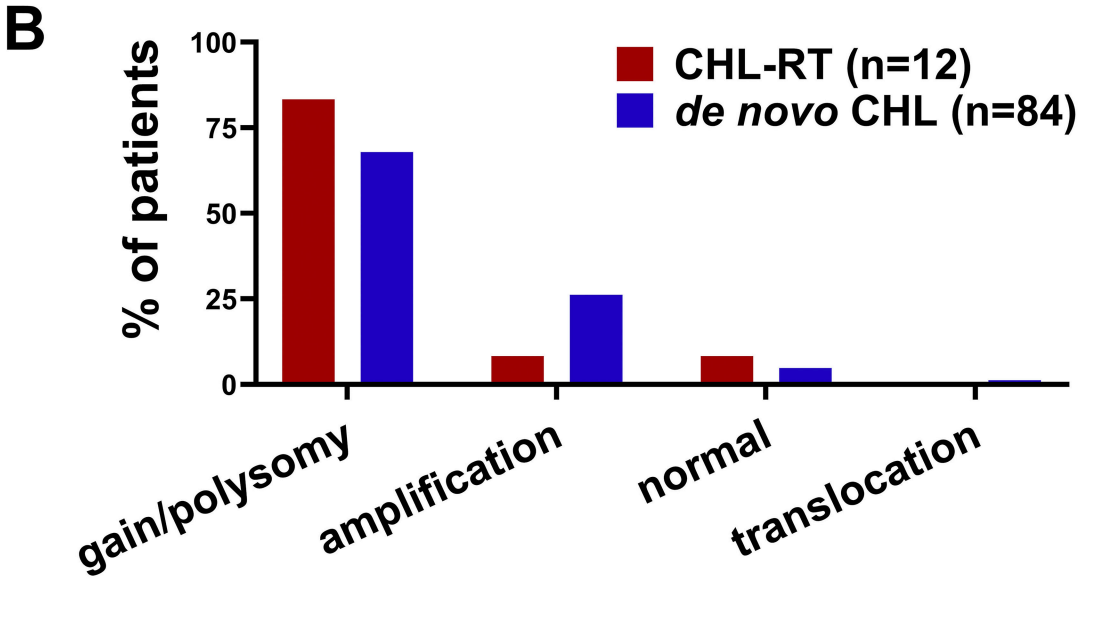

Type 1
Type 2
PAX5
CD30
PAX5
CD30

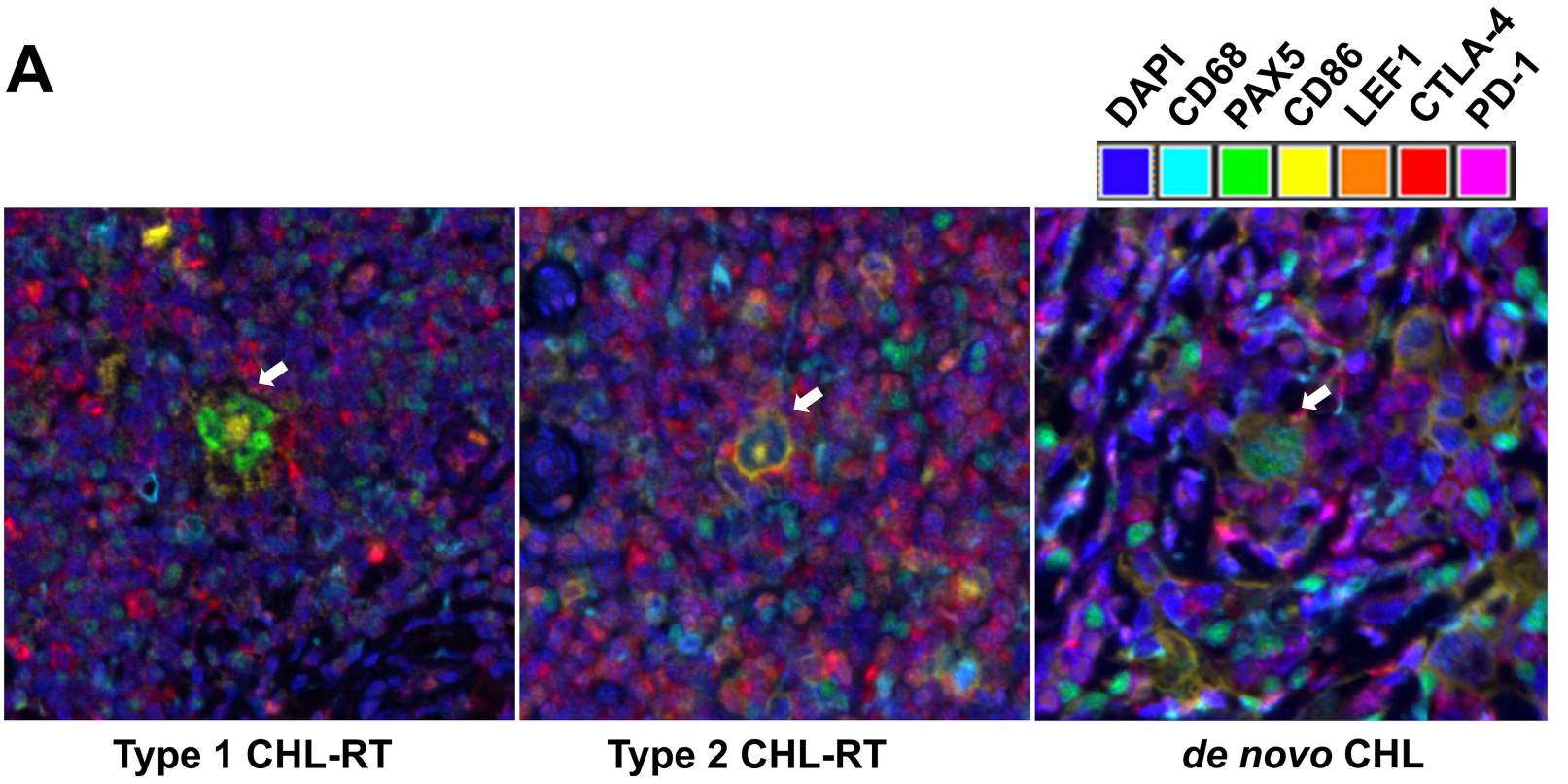
C

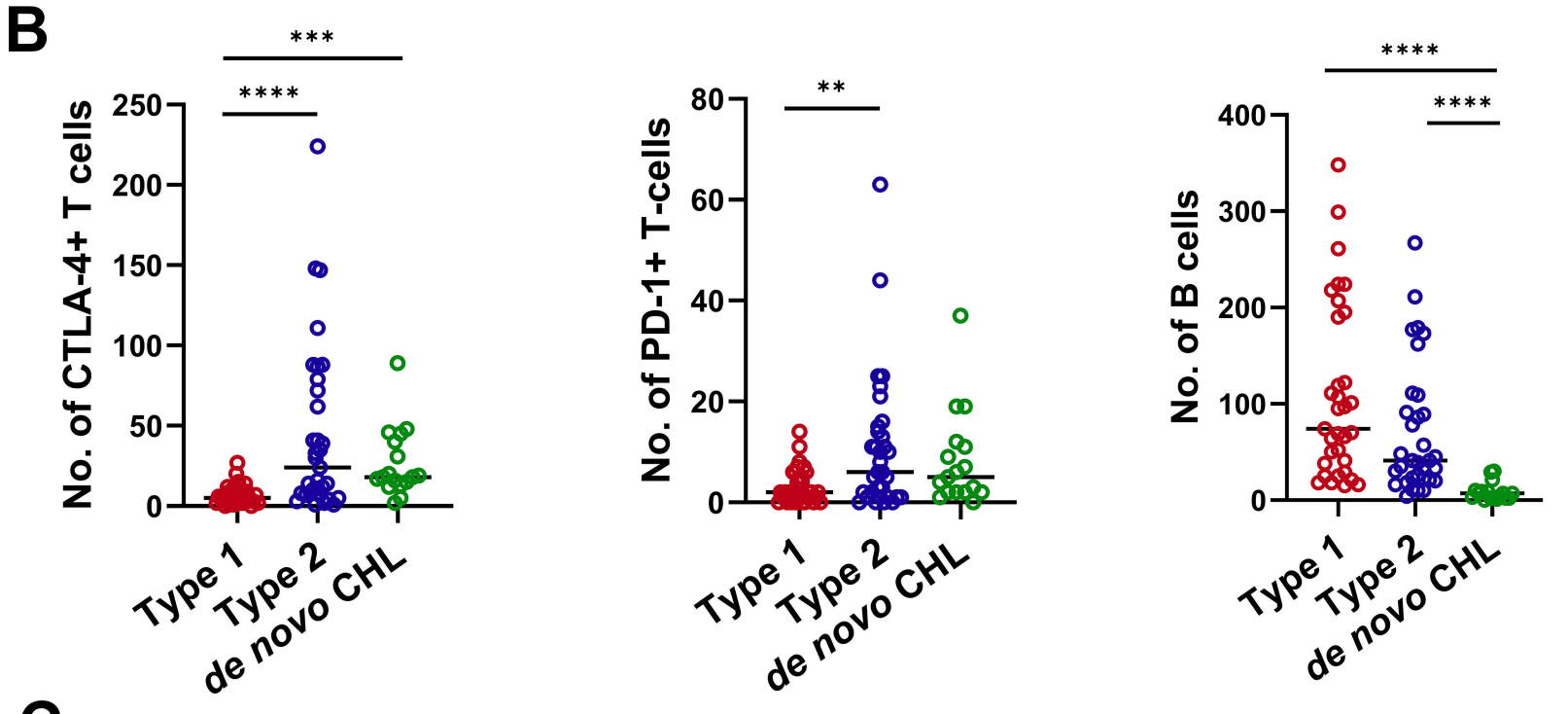

Type 1 CHL-RT
Type 2 CHL-RT
% of patients
100
75
50
25
0
CD30 (+)
CD15 (+)
PAX5 (dim)
CD20 (-)
CD45 (-)
EBER (+)

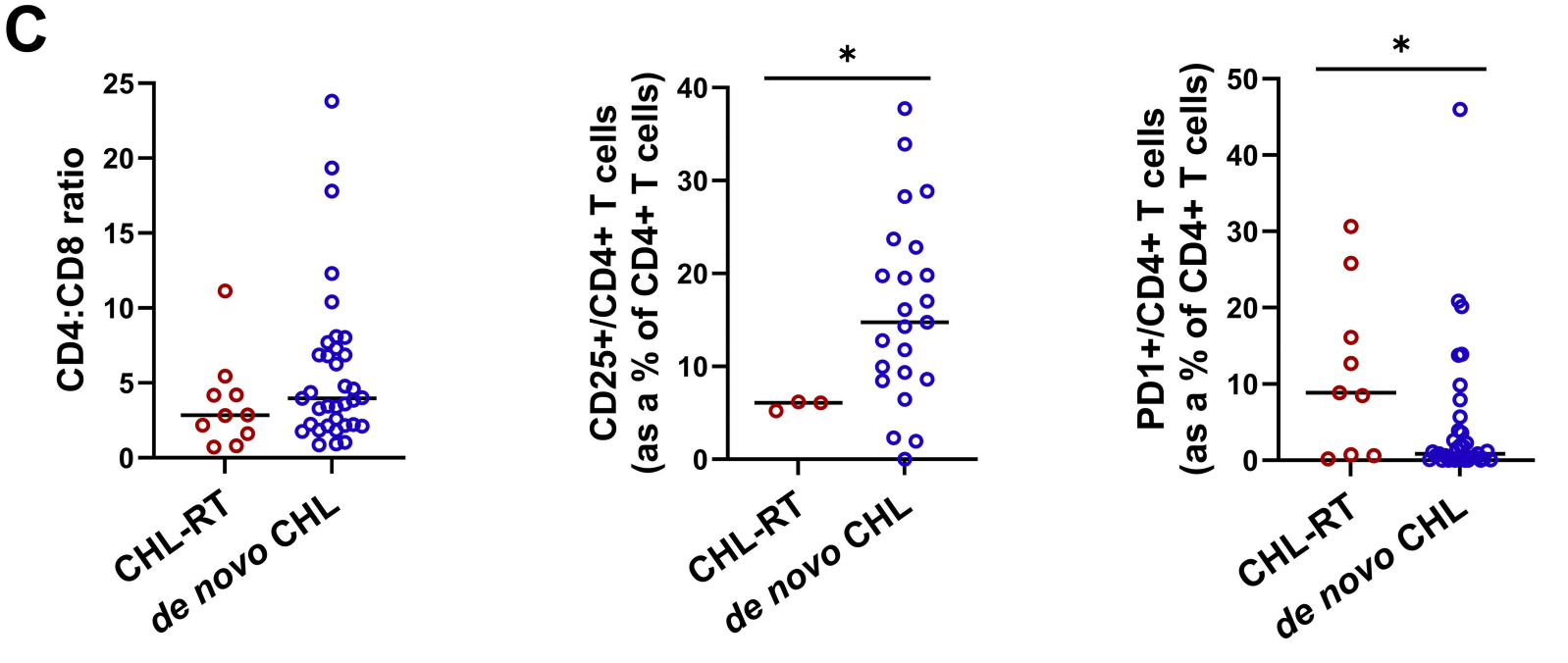

A
Positive
Negative
PD-L1
PD-L2
MHC-I
B2M
MHC-II
CIITA
B
Type 1 CHL-RT (n=15)
Type 2 CHL-RT (n=28)
de novo CHL (n=48)
% of patients
100
75
50
25
0
PD-L1 (+)
PD-L2 (+)
MHC-I (-)
B2M (-)
MHC-II (-)
CIITA (-)
EBER (+)
C
EBV-positive
Type 1 CHL-RT (n=10)
Type 2 CHL-RT (n=14)
de novo CHL (n=5)
% of patients
PD-L1 (+)
PD-L2 (+)
MHC-I (-)
B2M (-)
MHC-II (-)
CIITA (-)
EBV-negative
Type 1 CHL-RT (n=5)
Type 2 CHL-RT (n=9)
de novo CHL (n=23)
% of patients
PD-L1 (+)
PD-L2 (+)
MHC-I (-)
B2M (-)
MHC-II (-)
CIITA (-)

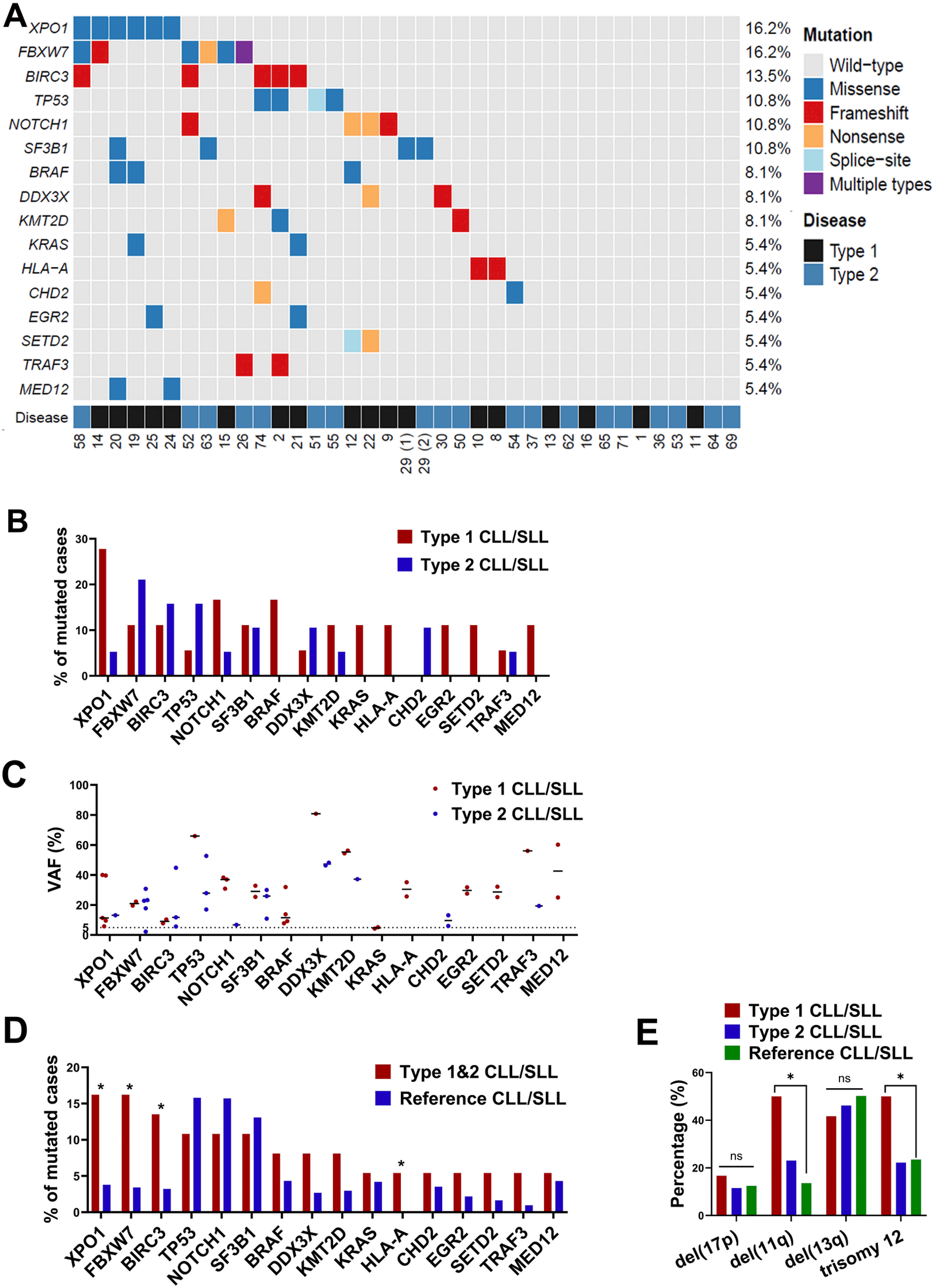

A
Normal
Polysomy
Gain
Amplification
red: PD-L1
green: PD-L2
blue: CD30
red: PD-L1
green: PD-L2
aqua: CEP9

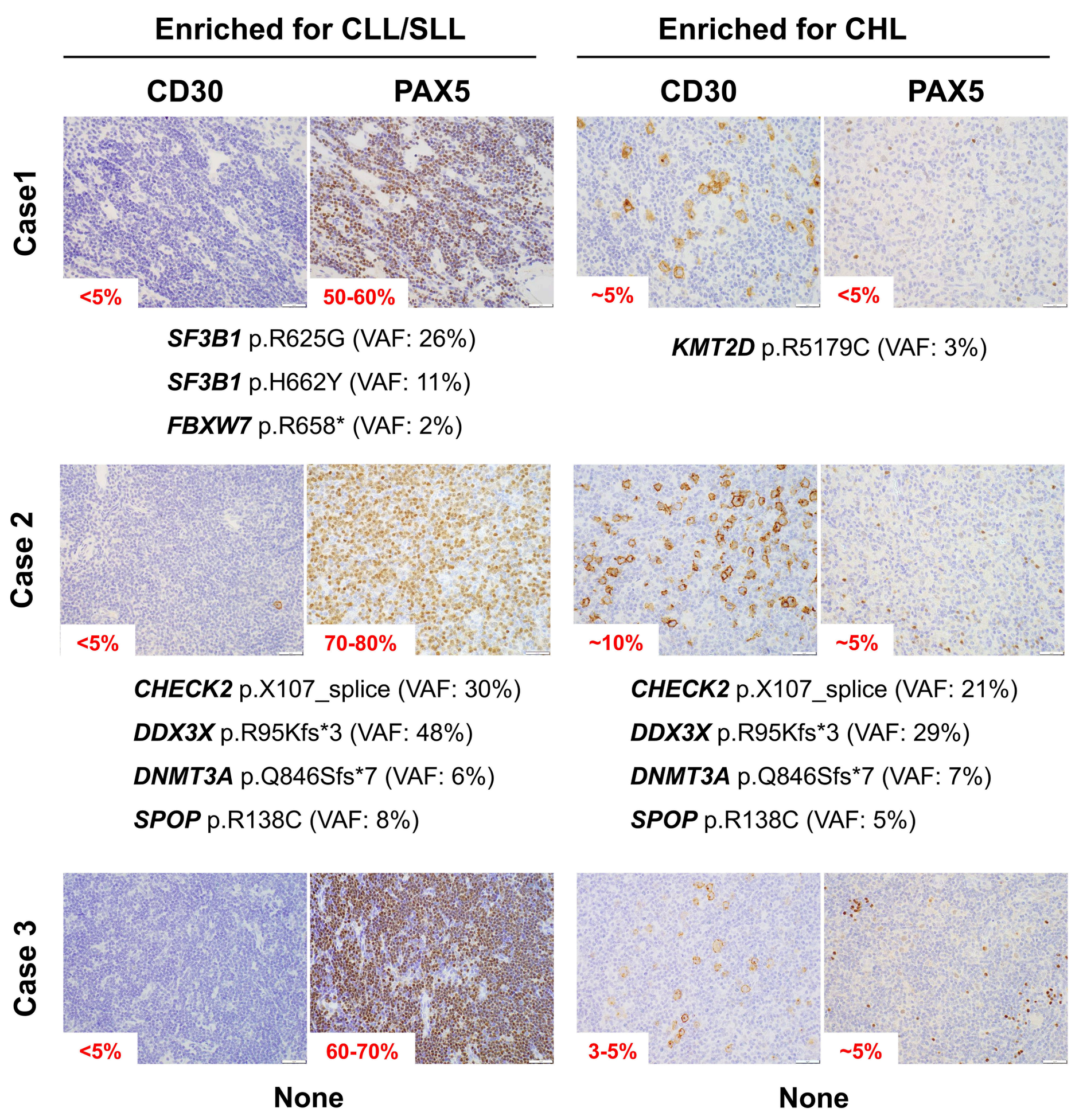

B
% of patients
100
75
50
25
0
CHL-RT (n=12)
de novo CHL (n=84)
gain/polysomy
amplification
normal
translocation

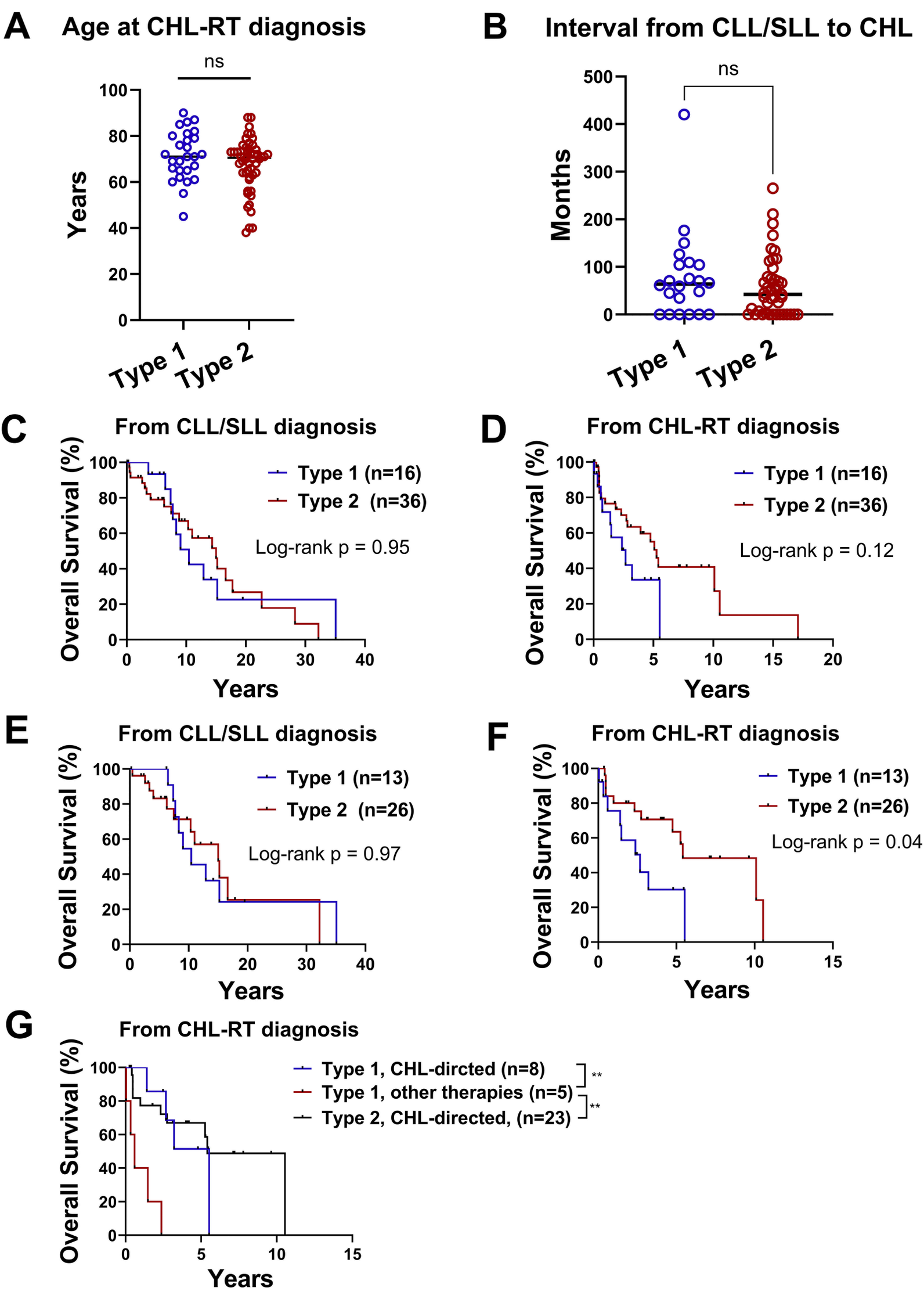

A
DAPI
CD68
PAX5
CD86
LEF1
CTLA-4
PD-1
Type 1 CHL-RT
Type 2 CHL-RT
de novo CHL


B
No. of CTLA-4+ T cells
No. of PD-1+ T-cells
No. of B cells
Type 1
Type 2
de novo CHL


C
CD4:CD8 ratio
CD25+/CD4+ T cells (as a % of CD4+ T cells)
PD1+/CD4+ T cells (as a % of CD4+ T cells)
CHL-RT
de novo CHL


A
XPO1
FBXW7
BIRC3
TP53
NOTCH1
SF3B1
BRAF
DDX3X
KMT2D
KRAS
HLA-A
CHD2
EGR2
SETD2
TRAF3
MED12
16.2%
16.2%
13.5%
10.8%
10.8%
10.8%
8.1%
8.1%
8.1%
5.4%
5.4%
5.4%
5.4%
5.4%
5.4%
Disease
58 14 20 19 25 24 52 63 15 26 74 2 21 51 55 12 22 9 29 (1) 29 (2) 30 50 10 8 54 37 13 62 16 65 71 1 36 53 11 64 69
Mutation
Wild-type
Missense
Frameshift
Nonsense
Splice-site
Multiple types
Disease
Type 1
Type 2
B
% of mutated cases
Type 1 CLL/SLL
Type 2 CLL/SLL
C
VAF (%)
Type 1 CLL/SLL
Type 2 CLL/SLL
D
% of mutated cases
Type 1&2 CLL/SLL
Reference CLL/SLL
E
Percentage (%)
Type 1 CLL/SLL
Type 2 CLL/SLL
Reference CLL/SLL
ns
ns
del(17p)
del(11q)
del(13q)
trisomy 12


Enriched for CLL/SLL
Enriched for CHL
CD30
PAX5
CD30
PAX5
Case1
<5%
50-60%
~5%
<5%
SF3B1 p.R625G (VAF: 26%)
SF3B1 p.H662Y (VAF: 11%)
FBXW7 p.R658* (VAF: 2%)
KMT2D p.R5179C (VAF: 3%)
Case 2
<5%
70-80%
~10%
~5%
CHECK2 p.X107_splice (VAF: 30%)
DDX3X p.R95Kfs*3 (VAF: 48%)
DNMT3A p.Q846Sfs*7 (VAF: 6%)
SPOP p.R138C (VAF: 8%)
CHECK2 p.X107_splice (VAF: 21%)
DDX3X p.R95Kfs*3 (VAF: 29%)
DNMT3A p.Q846Sfs*7 (VAF: 7%)
SPOP p.R138C (VAF: 5%)
Case 3
<5%
60-70%
3-5%
~5%
None
None


A
Age at CHL-RT diagnosis
ns
Years
100
80
60
40
20
0
Type 1
Type 2
B
Interval from CLL/SLL to CHL
ns
Months
500
400
300
200
100
0
Type 1
Type 2
C
From CLL/SLL diagnosis
Overall Survival (%)
Type 1 (n=16)
Type 2 (n=36)
Log-rank p = 0.95
Years
D
From CHL-RT diagnosis
Overall Survival (%)
Type 1 (n=16)
Type 2 (n=36)
Log-rank p = 0.12
Years
E
From CLL/SLL diagnosis
Overall Survival (%)
Type 1 (n=13)
Type 2 (n=26)
Log-rank p = 0.97
Years
F
From CHL-RT diagnosis
Overall Survival (%)
Type 1 (n=13)
Type 2 (n=26)
Log-rank p = 0.04
Years
G
From CHL-RT diagnosis
Overall Survival (%)
Type 1, CHL-dircted (n=8)
Type 1, other therapies (n=5)
Type 2, CHL-directed, (n=23)
**
**
Years

Supplementary table 1

Patient demographics, clinicopathologic characteristics, and ancillary testing

		Demographics					Ancillary tests			IHC and ISH results									Treatments and outcomes		
ID	CLL/SLL type	Sex	Age range at CLL/SLL dx	Age range at CHL-RT dx	HRS cell % in CLL/SLL	Months between CLL/SLL and CHL	NGS tested	FISH tested	mIF tested	EBER	CD30	CD15	PD-L1	PD-L2	MHC-I	B2M	MHC-II	CIITA	CLL treatment	CHL treatment	Outcome
1	Type 1	M	76-80	76-80	<5%	0	Yes	No	No	-	+	+	-	-	+	+	-	+	NA	NA	Alive
2	Type 1	F	61-65	76-80	<5%	176.4	Yes	No	Yes	+	+	-	NA	NA	NA	+	NA	+	PCR > ibrutinib	AVD + ibrutinib > ven + OB	Alive
3	Type 1	M	71-75	76-80	<5%	70.5	No	No	No	-	+	+	NA	NA	NA	NA	NA	NA	NA	R-CHOP > BR > ibrutinib > R-GCVP > palliative RT	Deceased
4	Type 1	F	81-85	86-90	~5%	66.3	No	No	No	NA	+	-	NA	NA	NA	NA	NA	NA	ibrutinib > observation	NA	Alive
5	Type 1	M	NA	71-75	<5%	NA	No	No	No	-	+	+	NA	NA	NA	NA	NA	NA	NA	NA	Alive
6	Type 1	M	NA	86-90	<5%	NA	No	No	No	-	+	-	NA	NA	NA	NA	NA	NA	NA	NA	Alive
7	Type 1	M	41-45	41-45	<5%	0	No	No	No	NA	+	+	NA	NA	NA	NA	NA	NA	NA	ABVD	Alive
8	Type 1	M	56-60	56-60	<5%	0	Yes	No	No	+	+	+	+	-	NA	-	-	+	NA	NA	NA
9	Type 1	F	86-90	86-90	<5%	0	Yes	No	No	-	+	+	-	NA	NA	NA	-	NA	NA	NA	NA
10	Type 1	M	NA	51-55	~5%	NA	Yes	No	No	+	+	+	+	-	+	+	+	+	NA	NA	NA
11	Type 1	M	56-60	61-65	<5%	109.6	Yes	No	No	+	+	-	-	-	NA	+	NA	+	NA	NA	NA
12	Type 1	M	56-60	56-60	<5%	48.7	Yes	No	No	+	+	+	+	-	+	+	+	-	NA	NA	NA
13	Type 1	M	66-70	66-70	<5%	0	Yes	No	Yes	+	+	-	-	-	+	+	+	+	NA	NA	NA
14	Type 1	F	NA	66-70	~5%	NA	Yes	Yes	No	-	+	+	-	-	+	+	+	+	NA	NA	NA
15	Type 1	M	NA	61-65	<5%	NA	Yes	No	No	-	+	+	+	-	+	+	+	+	NA	NA	NA
16	Type 1	M	NA	61-65	10-20%	NA	Yes	No	No	-	+	+	-	NA	NA	+	+	NA	NA	NA	NA
17	Type 1	F	66-70	71-75	<5%	104.3	No	No	No	+	+	-	NA	NA	NA	NA	NA	NA	NA	RT > BR > RT > BV + dacarbazine	Alive
18	Type 1	M	56-60	66-70	<5%	70.7	No	No	No	+	+	-	NA	NA	NA	NA	NA	NA	chlorambucil > fluda > CHOP > R > FC > DHAP > PCR > R + dex	R + MP > AR > MP > IT > R > ICE	Deceased
19	Type 1	F	61-65	66-70	<5%	59.2	Yes	No	No	+	+	+	+	-	+	+	-	+	PCR > IVIG > prednisone > R	ABVD > R > R + MP ibrutinib > BR > pembro > ibrutinib > R > len	Deceased
20	Type 1	M	66-70	71-75	~5%	150.3	Yes	Yes	Yes	+	+	-	-	-	+	+	+	+	R > PCR > CFAR > AR	ABVD > IVIG > ofatumumab > R + MP > BR > RT > dex > BV	Deceased
21	Type 1	M	66-70	71-75	<5%	75.7	Yes	No	No	+	+	+	+	-	-	+	+	+	AR > CpG > PCR	R + BV > BCVPP > BV > ABVD > R-GVP	Deceased
22	Type 1	M	81-85	81-85	<5%	34.8	Yes	No	No	+	+	-	NA	NA	NA	NA	NA	NA	NA	NA	Deceased
23	Type 1	M	46-50	81-85	<5%	420.4	No	No	No	+	+	-	NA	NA	NA	NA	NA	NA	chlorambucil	CHOP	Deceased
24	Type 1	M	71-75	81-85	<5%	126.4	Yes	No	No	-	+	+	NA	NA	NA	NA	NA	NA	AR > ibrutinib	MP > R > ibrutinib + ven	Deceased
25	Type 1	M	61-65	71-75	<5%	104.5	Yes	Yes	No	NA	+	+	+	-	-	+	+	+	PCR > BR	R > MP > CHOP	Deceased
26	Type 1	M	56-60	61-65	<5%	61.4	Yes	Yes	No	+	+	+	+	-	+	+	-	+	FCR > R	ABVD > ibrutinib > ICE > auto-SCT > ibrutinib >	Deceased

																			GVD > BV > nivolumab	
27	Type 1	M	71-75	76-80	<5%	45.2	No		No	+	+	-	NA	NA	NA	NA	NA	NA	ABVD > BV > acalabrutinib	Alive
28	Type 2	M	41-45	46-50	~10%	58.8	Yes	Yes	No	-	+	+	NA	NA	NA	NA	NA	+	PCR > CAR-T > RT > ibrutinib	ABVD > R + idelalisib > GCV > OB > benda + OB > allo-SCT > pembro	Alive
29 #	Type 2	M	61-65	61-65	<5%	0	Yes	No	No	+	+	-	NA	NA	NA	NA	NA	+	NA	R-EPOCH + ven > allo-SCT	Alive
30 *	Type 2	M	76-80	76-80	~5%	0.25	Yes	Yes	No	-	+	-	+	NA	NA	+	-	+	NA	AVD	Alive
31	Type 2	M	61-65	76-80	<5%	190.9	No	No	No	+	+	+	NA	NA	NA	NA	NA	NA	cytoxan > chlorambucil	NA	Deceased
32	Type 2	M	61-65	61-65	5-10%	0	No	No	No	NA	+	+	NA	NA	NA	NA	NA	NA	NA	ABVD > AVD	Alive
33	Type 2	M	46-50	46-50	5-10%	0	No	No	No	+	+	-	+	-	+	-	+	+	NA	NA	Deceased
34	Type 2	M	66-70	66-70	<5%	50.3	No	No	No	NA	+	+	+	-	+	+	-	+	acalabrutinib	BV-AVD > nivolumab + AD > ven + OB	Alive
35	Type 2	M	61-65	61-65	5-10%	0	No	No	No	NA	+	+	NA	NA	NA	NA	NA	NA	NA	BV > AVD > BV	Alive
36	Type 2	M	71-75	76-80	<5%	66.5	Yes	No	No	NA	+	-	+	-	+	+	+	+	observation	BV > AVD	Alive
37	Type 2	M	71-75	71-75	<5%	0	Yes	No	Yes	-	+	-	NA	NA	NA	NA	NA	+	NA	NA	Deceased
38	Type 2	F	61-65	61-65	<5%	0	No	No	No	+	+	+	NA	NA	NA	NA	NA	NA	NA	NA	Alive
39	Type 2	M	51-55	56-60	<5%	45.1	No	No	No	NA	+	-	+	-	+	NA	+	+	ibrutinib > R	BV + AVD	Alive
40	Type 2	M	36-40	36-40	<5%	0	No	No	No	+	+	+	NA	NA	NA	NA	NA	NA	NA	ABVD > RT	Alive
41	Type 2	F	61-65	66-70	<5%	56.7	No	No	No	NA	+	+	NA	NA	NA	NA	NA	NA	FCR > BR > ibrutinib	ABVD	Deceased
42	Type 2	M	86-90	86-90	<5%	12.1	No	No	No	-	+	+	NA	NA	NA	NA	NA	NA	NA	COPP > BV > ibrutinib	Deceased
43	Type 2	M	36-40	36-40	<5%	6.8	No	No	No	+	+	-	NA	NA	NA	NA	NA	NA	FCR	ABVD	Alive
44	Type 2	M	56-60	81-85	<5%	265.4	No	No	No	NA	+	+	NA	NA	NA	NA	NA	NA	bleomycin + CHOP > R	R-CEPP > BV > acalabrutinib	Deceased
45	Type 2	M	61-65	66-70	<5%	73	No	No	No	NA	+	+	NA	NA	NA	NA	NA	NA	observation	ABVD > GVD > allo-SCT > ibrutinib > ven	Deceased
46	Type 2	F	NA	36-40	5-10%	NA	No	No	No	NA	+	+	NA	NA	NA	NA	NA	NA	NA	NA	Alive
47	Type 2	M	71-75	71-75	<5%	2.8	No	No	No	-	+	-	NA	NA	NA	NA	NA	NA	NA	NA	Alive
48	Type 2	M	66-70	71-75	<5%	36.5	No	No	No	NA	+	-	NA	NA	NA	NA	NA	NA	ven + OB	BV > AVD > BV	Alive
49	Type 2	F	56-60	71-75	5-10%	166.3	No	No	No	+	+	+	NA	NA	NA	NA	NA	NA	ibrutinib > ven	benda + ibrutinib > AVD > BV	Alive
50	Type 2	M	66-70	71-75	~5%	36.5	Yes	No	No	-	+	+	+	-	NA	+	-	NA	NA	NA	NA
51	Type 2	F	66-70	66-70	~10%	36.5	Yes	Yes	No	-	+	+	+	-	+	+	-	+	NA	NA	NA
52	Type 2	M	66-70	66-70	<5%	0	Yes	No	No	+	+	+	+	-	+	+	+	+	NA	NA	NA
53	Type 2	M	71-75	71-75	~10%	0	Yes	Yes	No	-	+	+	+	-	-	+	+	+	NA	NA	NA
54	Type 2	M	NA	66-70	<5%	NA	Yes	No	No	+	+	+	+	NA	NA	+	-	+	NA	NA	NA
55	Type 2	F	NA	81-85	10-20%	NA	Yes	Yes	Yes	+	+	+	+	-	+	+	-	+	NA	NA	NA
56	Type 2	M	66-70	76-80	<5%	97.4	No	No	No	-	+	+	+	-	+	+	-	+	NA	NA	NA
57	Type 2	F	NA	61-65	<5%	NA	No	No	No	NA	+	+	+	-	+	+	+	+	NA	NA	NA
58	Type 2	M	66-70	71-75	<5%	24.4	Yes	No	No	+	+	+	+	-	+	NA	+	+	NA	NA	NA
59	Type 2	F	NA	71-75	20-30%	NA	Yes	Yes	No	+	+	+	+	NA	NA	-	+	NA	NA	NA	NA
60	Type 2	F	46-50	46-50	<5%	0	No	No	No	+	+	+	+	-	+	+	-	+	NA	NA	NA
61	Type 2	F	NA	56-60	<5%	NA	No	No	No	+	+	-	+	NA	NA	+	+	+	NA	NA	NA

62	Type 2	M	NA	71-75	~5%	NA	Yes	No	No	+	+	-	+	-	+	-	+	+	NA	NA	NA
63 *	Type 2	M	56-60	66-70	<5%	66.8	Yes	Yes	No	+	+	+	+	NA	NA	+	+	-	AR > CpG > FCR > PCR > pentostatin + AR	ABVD > ibrutinib	Alive
64	Type 2	M	46-50	51-55	<5%	58.5	Yes	No	No	+	+	+	+	-	+	+	+	+	CVP > fluda > CHOP > cytoxan > chlorambucil > R	NA	Deceased
65	Type 2	F	66-70	71-75	~10%	25.2	Yes	Yes	Yes	NA	+	+	+	-	+	+	+	+	NA	ABVD	Deceased
66	Type 2	F	61-65	71-75	<5%	134.2	No	No	No	+	+	+	NA	NA	NA	NA	NA	NA	NA	NA	Deceased
67	Type 2	M	61-65	61-65	<5%	0.1	No	No	No	+	+	-	NA	NA	NA	NA	NA	NA	NA	R + MP > ABVD	Deceased
68	Type 2	M	56-60	66-70	10-20%	117.5	Yes	No	No	+	+	+	+	+	+	-	+	+	R > PCR > CFAR > AR	ABVD > IVIG > ofatumumab > R + MP > BR > RT > dex > BV > dex	Deceased
69	Type 2	M	61-65	71-75	<5%	112.2	Yes	No	No	-	+	+	+	+	+	+	+	+	chlorambucil > fluda > R + MP > alemtuzumab	ABVD	Deceased
70	Type 2	M	71-75	81-85	<5%	117	No	No	No	+	+	+	NA	NA	NA	NA	NA	NA	NA	ABVD > R + MP > ABVD > BCVPP > R > prednisone > BR > ibrutinib > BR	Deceased
71 *	Type 2	M	71-75	76-80	<5%	42.4	Yes	No	No	-	+	-	+	NA	+	+	+	+	MP > obinutuzumab > chlorambucil	BV	Deceased
72	Type 2	M	41-45	51-55	<5%	138.2	No	No	No	+	+	+	NA	NA	NA	NA	NA	NA	fluda	NA	Deceased
73	Type 2	F	66-70	71-75	<5%	79.1	No	No	No	-	+	+	NA	NA	NA	NA	NA	NA	PCR + bevacizumab	BV + nivolumab > ABVD	Alive
74	Type 2	M	56-60	61-65	~5%	69.7	Yes	No	No	+	+	+	+	NA	NA	+	+	+	PCR > R + MP > R-CVP > prednisone	ABVD > IVIG > prednisone > ofatumumab > MP > ibrutinib > BV > BCVPP > ProMACE-cytaBOM	Deceased
75	Type 2	M	61-65	71-75	<5%	74.9	No	No	No	-	+	+	NA	NA	NA	NA	NA	NA	chlorambucil > prednisone > chlorambucil	CHOP > R + MP > fluda > AR	Deceased
76	Type 2	M	66-70	71-75	5-10%	33.9	No	No	No	-	+	+	+	-	+	+	+	+	fluda	NA	Deceased
77	Type 2	F	66-70	86-90	<5%	211	No	No	No	+	+	-	+	-	+	+	+	+	NA	NA	Deceased

Abbreviations: **ABVD**: doxorubicin, bleomycin, vinblastine, dacarbazine. **AD**: doxorubicin and dacarbazine. **Allo-SCT**: allogeneic stem cell transplantation. **AR**: alemtuzumab and rituximab. **Auto-SCT**: autologous stem cell transplantation. **AVD**: doxorubicin, vinblastine, dacarbazine. **BCVPP**: carmustine, cyclophosphamide, vinblastine, procarbazine, prednisone. **Benda**: bendamustine. **BR**: bendamustine and rituximab. **BV**: brentuximab vedotin. **CAR-T**: chimeric antigen receptor-T cell therapy. **CEPP**: cyclophosphamide, etoposide, procarbazine, and prednisone. **CFAR**: cyclophosphamide, fludarabine, alemtuzumab, and rituximab. **CHOP**: cyclophosphamide, doxorubicin, vincristine, and prednisone. **COPP**: cyclophosphamide, vincristine, procarbazine hydrochloride, and prednisone. **CpG**: CpG oligodeoxynucleotides. **CVP**: cyclophosphamide, vincristine, prednisolone. **Dex**: dexamethasone. **DHAP**: dexamethasone, high-dose cytarabine, and cisplatin. **EPOCH**: etoposide phosphate, prednisone, vincristine, cyclophosphamide, and doxorubicin. **FC**: fludarabine and cyclophosphamide**. FCR**: fludarabine, cyclophosphamide, and rituximab. **Fluda**: fludarabine. **GCV**: gemcitabine, cyclophosphamide, vincristine. **GCVP**: gemcitabine, cyclophosphamide, vincristine, prednisolone. **GVD**: gemcitabine, vincristine, and doxorubicin. **GVP**: gemcitabine, vincristine, prednisolone. **ICE**: ifosfamide, carboplatin, and etoposide. **IF**: immunofluorescence. **IHC**: Immunohistochemistry. **ISH**: In-situ hybridization. **IT**: ibritumomab tiuxetan. **IVIG**: intravenous immunoglobulin. **Len**: lenalidomide. **mIF**: multiplex immunofluorescence. **MP:** methylprednisolone. **OB**: obinutuzumab. **ProMACE-cytaBOM**: prednisone, methotrexate, Adriamycin, cyclophosphamide, etoposide, cytarabine, bleomycin, vincristine, methotrexate. **PCR**: pentostatin, cyclophosphamide, and rituximab. **Pembro**: Pembrolizumab**. R**: rituximab. **RT**: radiation therapy. **Ven**: venetoclax.

Note: # For this patient, two samples—one with type 1 and another with type 2 CLL/SLL—were submitted for NGS studies.

* NGS studies were conducted on macrodissected CLL/SLL-enriched and CHL-enriched areas separately for each of these patients.

Supplementary table 2

Gene list for MSK IMPACT-Heme

ABL1	*ACTG1*	*AKT1*	*AKT2*	*AKT3*	*ALK*	*ALOX12B*	*AMER1*	*APC*	*AR*
ARAF	*ARHGEF28*	*ARID1A*	*ARID1B*	*ARID2*	*ARID3A*	*ARID3B*	*ARID3C*	*ARID4A*	*ARID4B*
ARID5A	*ARID5B*	*ASXL1*	*ASXL2*	*ATM*	*ATP6AP1*	*ATP6V1B2*	*ATR*	*ATRX*	*ATXN2*
AURKA	*AURKB*	*AXIN1*	*AXL*	*B2M*	*BACH2*	*BAP1*	*BARD1*	*BCL10*	*BCL11B*
BCL2	*BCL6*	*BCOR*	*BCORL1*	*BCR*	*BIRC3*	*BLM*	*BRAF*	*BRCA1*	*BRCA2*
BRD4	*BRIP1*	*BTG1*	*BTK*	*CALR*	*CARD11*	*CASP8*	*CBFB*	*CBL*	*CCND1*
CCND2	*CCND3*	*CCNE1*	*CD274*	*CD28*	*CD58*	*CD79A*	*CD79B*	*CDC73*	*CDH1*
CDK12	*CDK4*	*CDK6*	*CDK8*	*CDKN1B*	*CDKN2A*	*CDKN2B*	*CDKN2C*	*CEBPA*	*CHEK1*
CHEK2	*CIC*	*CIITA*	*CRBN*	*CREBBP*	*CRKL*	*CRLF2*	*CSF1R*	*CSF3R*	*CTCF*
CTNNB1	*CUX1*	*CXCR4*	*CYLD*	*DAXX*	*DDR2*	*DDX3X*	*DIS3*	*DNMT3A*	*DOT1L*
DTX1	*DUSP22*	*EED*	*EGFR*	*EGR1*	*EP300*	*EP400*	*EPHA3*	*EPHA5*	*EPHA7*
EPHB1	*ERBB2*	*ERBB3*	*ERBB4*	*ERG*	*ESCO2*	*ESR1*	*ETNK1*	*ETV6*	*EZH2*
FANCA	*FANCC*	*FANCD2*	*FAS*	*FAT1*	*FBXO11*	*FBXW7*	*FGF19*	*FGF3*	*FGF4*
FGFR1	*FGFR2*	*FGFR3*	*FGFR4*	*FLCN*	*FLT1*	*FLT3*	*FLT4*	*FOXL2*	*FOXO1*
FOXP1	*FURIN*	*FYN*	*GATA1*	*GATA2*	*GATA3*	*GNA11*	*GNA12*	*GNA13*	*GNAQ*
GNAS	*GNB1*	*GRIN2A*	*GSK3B*	*H1-2*	*H2BC5*	*H3C2*	*H3C8*	*HDAC1*	*HDAC4*
HDAC7	*HGF*	*HIF1A*	*HIST1H1B*	*HIST1H1D*	*HIST1H1E*	*HIST1H2AC*	*HIST1H2AG*	*HIST1H2AL*	*HIST1H2AM*
HIST1H2BC	*HIST1H2BG*	*HIST1H2BJ*	*HIST1H2BK*	*HIST1H2BO*	*HLA-A*	*HNF1A*	*HRAS*	*ID3*	*IDH1*
IDH2	*IGF1*	*IGF1R*	*IGF2*	*IKBKE*	*IKZF1*	*IKZF3*	*IL7R*	*INPP4B*	*IRF1*
IRF4	*IRF8*	*IRS2*	*JAK1*	*JAK2*	*JAK3*	*JARID2*	*JUN*	*KDM5A*	*KDM5C*
KDM6A	*KDR*	*KEAP1*	*KIT*	*KMT2A*	*KMT2B*	*KMT2C*	*KMT2D*	*KMT5A*	*KRAS*
KSR2	*LCK*	*LMO1*	*LTB*	*MALT1*	*MAP2K1*	*MAP2K2*	*MAP2K4*	*MAP3K1*	*MAP3K13*
MAP3K14	*MAPK1*	*MAPK3*	*MCL1*	*MDM2*	*MDM4*	*MED12*	*MEF2B*	*MEN1*	*MET*
MGA	*MGAM*	*MITF*	*MLH1*	*MOB3B*	*MPEG1*	*MPL*	*MRE11*	*MSH2*	*MSH6*
MTOR	*MUTYH*	*MYC*	*MYCL*	*MYCN*	*MYD88*	*NBN*	*NCOR1*	*NCOR2*	*NCSTN*
NF1	*NF2*	*NFE2*	*NFE2L2*	*NKX2-1*	*NOTCH1*	*NOTCH2*	*NOTCH3*	*NOTCH4*	*NPM1*
NRAS	*NSD1*	*NT5C2*	*NTRK1*	*NTRK2*	*NTRK3*	*P2RY8*	*PAK7*	*PALB2*	*PARP1*
PAX5	*PBRM1*	*PCBP1*	*PDCD1*	*PDGFRA*	*PDGFRB*	*PDPK1*	*PDS5B*	*PHF6*	*PIGA*
PIK3C2G	*PIK3C3*	*PIK3CA*	*PIK3CG*	*PIK3R1*	*PIK3R2*	*PIM1*	*PLCG1*	*PLCG2*	*PMS2*
PNRC1	*POT1*	*PPP2R1A*	*PRDM1*	*PRKAR1A*	*PTCH1*	*PTEN*	*PTPN1*	*PTPN11*	*PTPN2*
RAD21	*RAD50*	*RAD51*	*RAD51B*	*RAD51C*	*RAD51D*	*RAD52*	*RAD54L*	*RAF1*	*RARA*
RB1	*REL*	*RET*	*RHOA*	*RICTOR*	*RNF43*	*ROBO1*	*ROS1*	*RPTOR*	*RRAGC*
RTEL1	*RUNX1*	*RUNX1T1*	*SAMHD1*	*SDHA*	*SDHB*	*SDHC*	*SDHD*	*SETBP1*	*SETD1A*
SETD1B	*SETD2*	*SETD3*	*SETD4*	*SETD5*	*SETD6*	*SETD7*	*SETDB1*	*SETDB2*	*SF3B1*
SGK1	*SH2B3*	*SMAD2*	*SMAD4*	*SMARCA4*	*SMARCB1*	*SMARCD1*	*SMC1A*	*SMC3*	*SMG1*
SMO	*SOCS1*	*SOX2*	*SP140*	*SPEN*	*SPOP*	*SRC*	*SRSF2*	*STAG1*	*STAG2*
STAT3	*STAT5A*	*STAT5B*	*STAT6*	*STK11*	*SUFU*	*SUZ12*	*SYK*	*TBL1XR1*	*TBX3*
TENT5C	*TERT*	*TET1*	*TET2*	*TET3*	*TGFBR2*	*TNFAIP3*	*TNFRSF14*	*TOP1*	*TP53*
TP53	*TP63*	*TRAF2*	*TRAF3*	*TRAF5*	*TSC1*	*TSC2*	*TSHR*	*TYK2*	*U2AF1*
U2AF2	*UBR5*	*VAV1*	*VAV2*	*VHL*	*WHSC1*	*WT1*	*XBP1*	*XPO1*	*ZRSR2*

Supplementary materials and methods

Patient cohort

CHL-RT diagnoses were identified over a study period extending from 1995 to 2022 (8 cases were diagnosed between 1995 and 2004, 30 cases between 2005 and 2014, and 39 cases between 2015 and 2025). Patients were allocated into type 1 and type 2 CHL-RT groups based on the diagnoses rendered by one of three pathologists (ESJ, RK, or WX). All cases subsequently underwent blinded central pathology review by YM and WX for diagnostic confirmation. This cohort included 27 type 1 and 50 type 2 patients, with ten of the type 2 patients exhibiting pathology samples that showed only CHL without morphological and immunophenotypic evidence of previously diagnosed CLL/SLL. Among the 50 type 2 CHL-RT, 43 cases were diagnosed with lymph node biopsies, and the remaining 7 cases were diagnosed with bone marrow biopsies. Notably, four patients demonstrated both type 1 and type 2 diseases in separate pathological samples; for the purposes of this study, these patients were classified as having type 2 diseases. Detailed information on patient numbers from each contributing institution is shown in Figure 1A. No publicly deposited datasets were generated or used in this study. No animals were used in this study.

Immunohistochemistry (IHC) and in situ hybridization (ISH)

The following antibodies or probe were used: PD-L1 (clone: E1L3N), PD-L2 (clone: D7U8C), MHC-I (clone: A4), B2M (clone: A0072), HLA-DR (MHC-II) (clone: TAL 1B5), CIITA (clone: 7-1H), EBV-encoded RNA (EBER) ISH (Ventana, 760-1209). Appropriate positive and negative controls were included and confirmed for all antibodies.

Multiplexed immunofluorescence (mIF)

Heat-induced epitope retrieval (HIER) was conducted using Epitope Retrieval Solution 2 (ER2, Leica) for 30 minutes. Each primary antibody—CD68 (clone PM-G1, Agilent Technologies), PAX5 (clone D7H5X, Cell Signaling Technology), CD86 (clone E2G8P, Cell Signaling Technology), CTLA-4 (clone CAL49, abcam), LEF1 (clone EPR2029Y, abcam), and PD-1 (clone NAT105, Millipore Sigma) —was applied sequentially for 30 minutes at room temperature. Antibody dilutions were optimized through prior titration on normal and neoplastic control tissues. Secondary detection employed species-specific SuperBoost™ Poly HRP antibodies (ThermoFisher), followed by tyramide signal amplification using the Opal 6-Plex Detection Kit (Akoya Biosciences). After each round, antibodies were stripped via HIER with ER2. Slides were counterstained with 4′,6-diamidino-2-phenylindole (DAPI) and mounted using ProLong™ Gold antifade reagent (ThermoFisher). mIF-stained slides were scanned at 20× magnification using a PhenoImager (Akoya/Quanterix) whole-slide scanner. Whole-slide images were imported into the HALO image analysis platform (version (4.0), Indica Lab). Cell segmentation was performed using the HALO (Nuclei Seg V2) module, with nuclei identified based on DAPI staining. Marker positivity thresholds were established using internal positive and negative controls and applied uniformly across all samples. Subsequently,

150 × 150 μm regions of interest (ROIs) centered on Hodgkin and Reed-Sternberg (HRS) cells were manually annotated to evaluate the tumor microenvironment within a 75 μm radius. HRS cells were identified based on nuclear size and morphology, as well as expression of CD86. Quantitative outputs, including the number of PD-1$^+$ T cells (defined by co-expression of LEF1 and PD-1 in the absence of all other markers), CTLA-4$^+$ T cells (defined by co-expression of LEF1 and CTLA-4 in the absence of all other markers), B cells (defined by expression of PAX5), and histiocytes (defined by expression of CD68) within ROIs, were exported for downstream statistical analysis. None of the CHL-RT cases analyzed by mIF had both type 1 and type 2 diseases in separate pathological samples.

Flow cytometric analysis

Flow cytometric studies were performed on all samples in a standard manner as part of routine clinical practice at MSKCC. Tissue biopsy specimens were finely minced in RPMI 1640 growth medium using scalpel blades, then filtered and resuspended in RPMI. Needle aspirates and biopsy needle rinses were suspended in RPMI. Cells in RPMI were then stained with a 21-antibody assay (CD2, CD3, CD4, CD5, CD7, CD8, CD10, CD14, CD19, CD20, CD22, CD25, CD26, CD38, CD45, CD56, CD279 (PD-1), TCRγδ, TCRCβ1, Kappa, Lambda) designed to evaluate both B and T cells. Due to availability and periodic changes in clinical laboratory protocols, some cases were stained with only portions of this modular panel separately. Following staining and incubation, cells were lysed, fixed, washed, and resuspended. Up to 500,000 cells were acquired on a Fluorescence-activated cell sorting (FACS) Canto 10 color flow cytometer (BD), BD LSR Fortessa X-20 20 color flow cytometer (BD), or BD FACSymphony A3 28 color flow cytometer (BD). Results were analyzed with custom Woodlist software (generous gift of Wood BL, Children's Hospital of Los Angeles, Los Angeles, CA, USA). All assays were initially assessed by a single pathologist (A.C.).

Combined CD30 immunofluorescence and *PD-L1/PD-L2* FISH analysis

Following immunophenotyping with mouse anti-CD30 antibody (clone: Ber-H2) labeled with aminomethylcoumarin acetate (AMCA), a blue fluorescent dye, the tissue slides with coverslips were briefly reviewed and documented under a fluorescence microscope to assess the intensity and quality of CD30 staining. After removing the coverslips, the slides were washed in 2× saline-sodium citrate (SSC) buffer at room temperature for 5 minutes, then fixed in 10% neutral buffered formalin for 20 minutes. The slides were subsequently dehydrated in ascending alcohol concentrations (70%, 85%, and 100%) for 5 minutes each. Next, the slides underwent pretreatment with a 20 mM citrate buffer and 1% NP-40 mixture (pH 6.0-6.5) for 10 minutes, followed by protease digestion at 40°C for 10-15 minutes (Abbott Molecular, Des Plaines, IL). The dehydration process was repeated with 2-minute immersions in 70%, 85%, and 100% alcohol. For fluorescence in situ hybridization (FISH), probes for *PD-L1* (Spectrum Orange) and *PD-L2* (Spectrum Green) (both from Empire Genomics, Buffalo, NY) were used, along with *CEP9* (Spectrum Aqua) (Abbott Molecular, Des Plaine, IL) as an internal control for chromosome 9 copy number (all from Genomic Empire, Buffalo, NY). FISH testing follows the standard protocol. Briefly, after applying

the FISH probes to the tissue areas, both tissue and probes were co-denatured at 94º C for 7 minutes, and then incubated at 37º C overnight, followed by post-hybridization washing in 2xSSC/0.3% NP-40 at 77º C for one minute. The sections were counterstained with an antifade medium lacking DAPI (Vector Laboratories, Burlingame, CA). Slides were examined under a fluorescence microscope equipped with appropriate filters for CD30 immunofluorescence and *PD-L1/PD-L2* and *CEP9* probes.

Next-generation sequencing (NGS)

The NGS was performed by MSK-IMPACT (Integrated Mutation Profiling of Actionable Cancer Targets)-Heme assay, a hybrid-capture-based platform designed to capture all canonical exons of 400 key oncogenes and tumor suppressor genes implicated in hematologic malignancies. This includes genes that are either druggable by approved therapies or are targets of experimental therapies currently under investigation in clinical trials at our institution. Unlike the paired sequencing approach used in routine clinical practice, which incorporates matched normal tissue to distinguish somatic from germline variants, the NGS analyses in this study were performed without matched normal controls. Consequently, germline variants and patient-specific single nucleotide polymorphisms (SNPs) may be present in the data.

NGS was performed on bulk CLL/SLL FFPE tissue from 17 patients with type 1 CHL-RT and 15 patients with type 2 CHL-RT, two separate bulk CLL/SLL FFPE tissue from a patient who exhibited either type 1 or type 2 CHL-RT in different samples, and bulk FFPE tissue from three patients with type 2 CHL-RT with samples showing only CHL with a high density of HRS cells (comprising more than 10% cellularity) but no morphologic and flow cytometric evidence of previously diagnosed CLL/SLL. In addition, macrodissection was performed on samples from three patients with type 2 CHL-RT who displayed distinct areas that were enriched for either CLL/SLL or CHL, allowing for separate analysis of the CLL/SLL and CHL components. In total, NGS was performed on 43 samples from 39 patients, comprising 18 CLL/SLL samples from type 1 CHL-RT, 19 CLL/SLL samples from type 2 CHL-RT, and 6 CHL-enriched samples from type 2 CHL-RT.

Statistical analysis

Numerical data were analyzed using Student's t-test. Categorical data were compared by Fisher’s exact test. Overall survival was calculated from the initial date of diagnosis until the date of death or last follow-up. Survival data were visualized using Kaplan-Meier curves and analyzed with the two-sided log-rank (Mantel-Cox) test. The statistical analysis was performed using GraphPad Prism (RRID:SCR_002798) or R (version 4.2.2). The oncoplot was generated by ggplot2 (RRID:SCR_014601) in R (version 4.2.2). Statistical significance was defined as a p-value less than 0.05. Given the rarity of the disease, all eligible patients identified during the study period were included. No formal sample size calculation was performed, as the cohort size was constrained by case availability.